NREL/TP-411-5289 • UC Category: 275 • DE93000073

An Inverted AlGaAs/GaAs Patterned-Ge Tunnel Junction Cascade Concentrator Solar Cell

Final Subcontract Report
1 January 1991 – 31 August 1992

NREL/TP--411-5289

DE93 000073

R. Venkatasubramanian
Research Triangle Institute
Research Triangle Park, North Carolina

NREL technical monitor: T. S. Basso

National Renewable Energy Laboratory
1617 Cole Boulevard
Golden, Colorado 80401-3393
A Division of Midwest Research Institute
Operated for the U.S. Department of Energy
under Contract No. DE-AC02-83CH10093

Prepared under Subcontract No. XM-0-18110-2

January 1993

MASTER

DISTRIBUTION OF THIS DOCUMENT IS UNLIMITED

NOTICE

This report was prepared as an account of work sponsored by an agency of the United States government. Neither the United States government nor any agency thereof, nor any of their employees, makes any warranty, express or implied, or assumes any legal liability or responsibility for the accuracy, completeness, or usefulness of any information, apparatus, product, or process disclosed, or represents that its use would not infringe privately owned rights. Reference herein to any specific commercial product, process, or service by trade name, trademark, manufacturer, or otherwise does not necessarily constitute or imply its endorsement, recommendation, or favoring by the United States government or any agency thereof. The views and opinions of authors expressed herein do not necessarily state or reflect those of the United States government or any agency thereof.

Printed in the United States of America
Available from:
National Technical Information Service
U.S. Department of Commerce
5285 Port Royal Road
Springfield, VA 22161

Price: Microfiche A01
Printed Copy A05

Codes are used for pricing all publications. The code is determined by the number of pages in the publication. Information pertaining to the pricing codes can be found in the current issue of the following publications which are generally available in most libraries: *Energy Research Abstracts (ERA)*; *Government Reports Announcements* and Index (*GRA* and I); *Scientific and Technical Abstract Reports (STAR)*; and publication NTIS-PR-360 available from NTIS at the above address.

DISCLAIMER

Portions of this document may be illegible electronic image products. Images are produced from the best available original document.

FOREWORD

The work described in this report was done at the Center for Semiconductor Research of the Research Triangle Institute. Dr. R. Venkatasubramanian was the RTI Project Leader. The project leader would like to acknowledge the significant contributions of Dr. M.L. Timmons, Mr. T.S. Colpitts, Ms. J.S. Hills and Dr. J.A. Hutchby during the past two years on this effort. Dr. P.R. Sharps and Mr. J. Hancock are also acknowledged for their technical support. Ms. G.B. Peed and Ms. K. Barbour have provided secretarial support.

The project leader is pleased to acknowledge and thank several NREL personnel who have provided technical support. We sincerely appreciate the help of Dr. Keith Emery with solar cell data, Dr. R.K. Ahrenkiel with photoluminescence decay lifetime data, and Dr. S. Asher with secondary ion mass spectroscopy measurements. We also thank the encouragement and support of our technical contract monitor, Mr. T.S. Basso.

TABLE OF CONTENTS

1.0 HIGHLIGHTS 1

2.0 INTRODUCTION 3

3.0 $Al_{0.34}Ga_{0.66}As$ TOP CELL DEVELOPMENT 7

4.0 GaAs TUNNEL JUNCTIONS FOR INVERTED-GROWN CASCADES .. 13

5.0 EUTECTIC METAL BONDING 19

6.0 INVERTED-GROWN GaAs THIN FILM SOLAR CELLS 27

7.0 THIN-FILM $Al_{0.34}Ga_{0.66}As$/GaAs CASCADES 33

8.0 SUMMARY AND CONCLUSIONS 35

9.0 PUBLICATIONS 37

10. REFERENCES 39

11. APPENDIX 1 41

LIST OF FIGURES

FIGURE 1: Schematic of the inverted-grown AlGaAs/GaAs cascade employing a planar GaAs tunnel junction interconnect. 4

FIGURE 2: Schematic of a current-matched, 3-junction cascade that can be developed using the concept of eutectic metal bonding (EMB) of a monolithic AlGaAs/GaAs cascade or a $GaInP_2$/GaAs cascade to an active Si cell. 5

FIGURE 3: Schematic of the $Al_{0.34}Ga_{0.66}As$ top cell being developed for the inverted AlGaAs/GaAs cascade. 8

FIGURE 4: Spectral response of $Al_{0.34}Ga_{0.66}As$ (a) cell with a 3.5 µm-base a and 500 Å $Al_{0.8}Ga_{0.2}As$ window and (b) cell with a 2 µm-base and 300 Å $Al_{0.8}Ga_{0.2}As$ window. 9

FIGURE 5a: I/V data on an $Al_{0.34}Ga_{0.66}As$ cell with a base thickness of 3.5 µm and an $Al_{0.8}Ga_{0.2}As$ window of 500Å thickness. 10

FIGURE 5b: I/V data on an $Al_{0.34}Ga_{0.66}As$ cell with a base thickness of 2.0 µm, compatible with the inverted growth of the cell at 780C. 11

FIGURE 6: Schematic of a typical GaAs tunnel junction with the various layer specifications used to evaluate the use of cycled growth. 14

FIGURE 7: I/V characteristics of GaAs tunnel junctions grown with continuous growth for GaAs:Se, and (a) continuous and (b) cycled growth for GaAs:Zn. Shown in (c) is the I/V characteristic for a tunnel junction with cycled growth for GaAs:Se and GaAs:Zn. 15

FIGURE 8: I/V characteristics of tunnel junctions with GaAs:Si for the n^+- regions and (a) continuous growth and (b) cycled growth for GaAs:Zn. 17

FIGURE 9: Schematic of a GaAs tunnel junction including the $Al_{0.8}Ga_{0.2}As$ hetero-barriers for improved thermal stability during the inverted growth of the GaAs bottom cell. 18

FIGURE 10: Phase diagrams of the a) Au-Si and b) Au-Ga-As systems, indicating the formation of the Si-Au eutectic and a range of AuGa eutectics at 400°C (from Ref. 13). 20

FIGURE 11: Schematic of the steps to produce EMB AlGaAs/GaAs thin films on Si. 21

FIGURE 12: Raman Spectrum from an EMB GaAs thin film on Si, obtained using an Ar^+ ion laser excitation at 514.5 nm. 22

FIGURE 13: 300 K PL spectra from an EMB GaAs thin film obtained from (a) the GaAs buffer originally adjacent to the Ge substrate, (b) the GaAs active layer after the selective removal of the GaAs buffer. 24

Figure 14: 300K PL decay from an EMB GaAs/AlGaAs DH structure on Si 25

FIGURE 15: I/V data on an EMB thin-film GaAs solar cell on Si 28

FIGURE 16 Spectral-response data on an EMB thin-film GaAs solar cell on Si. 29

FIGURE 17: I-V characteristic of a thin-film, inverted-grown, $Al_{0.34}Ga_{0.66}As/GaAs$ cascade under AM1.5D spectrum. 34

LIST OF TABLES

TABLE 1: Peak tunnel current density of GaAs tunnel junctions at different growth temperatures, using continuous and cycled growths for GaAs:Zn. 18

TABLE 2: Effect of solar concentration on cascade parameters. 34

1.0 HIGHLIGHTS

The significant developments for the second year of this program to develop inverted-grown $Al_{0.34}Ga_{0.66}As/GaAs$ cascades are the following:

- The AM1.5 1-sun total-area efficiency of the top $Al_{0.34}Ga_{0.66}As$ cell for the cascade was improved from 11.3% (at the end of first year of this program) to 13.2% (NREL measurement*). This represents a 1-sun active-area efficiency of 15.2%, an improvement from 13.7% at the end of last year.

- The "cycled" organometallic vapor phase epitaxy (OMVPE) growth (used to obtain significant enhancement in the conductance of GaAs tunnel junctions in the first year of this program) was studied in detail utilizing a combination of characterization techniques including Hall-data, photoluminescence, and secondary ion mass spectrometry.

- A technique called eutectic-metal-bonding (EMB) has been developed for strain-free mounting of thin GaAs-AlGaAs films (based on lattice-matched growth on Ge substrates and selective plasma etching of Ge substrates, developed in the first year of this program) onto Si carrier substrates. Minority-carrier lifetime in an EMB GaAs double-heterostructure has been measured to be as high as 103 nsec, the highest lifetime reported for a freestanding GaAs thin film.

- A thin film, inverted-grown, GaAs cell with a 1-sun AM1.5 active-area efficiency of 20.3% has been obtained. This inverted-grown, thin-film cell was eutectic-metal-bonded onto Si.

- A thin film, inverted-grown, $Al_{0.34}Ga_{0.66}As/GaAs$ cascade with AM1.5 efficiency of 19.9% and 21% at 1-sun and 7-suns, respectively, has been obtained. This cascade represents an important milestone in the development of

---

* NREL measures total-area efficiencies. Active area values are based on RTI measurements and may be more appropriate for cells designed for concentrators.

an AlGaAs/GaAs cascade by OMVPE utilizing a tunnel interconnect and demonstrates a proof-of-concept for the inverted-growth approach.

2.0 INTRODUCTION

Monolithic $Al_{0.37}Ga_{0.63}As$/GaAs (1.90 eV/1.43 eV bandgap pair) solar cells, based on a lattice-matched AlGaAs/GaAs material system with a mature growth technology and near-ideal current-match of component cells, can offer high efficiency ($\geq$ 30%) in concentrator-based (~ 500 suns) terrestrial photovoltaic applications. The key impediment for achieving high-efficiency cascade cells has been the high growth temperature (~780°C) required for high quality AlGaAs. The high temperatures deteriorate the conductance of the intercell ohmic connection. A successful approach to the $Al_{0.37}Ga_{0.63}As$/GaAs cascade has been the use of a metal interconnect [1] between the component cells as part of post-growth cell processing. This structure has demonstrated an efficiency of 27.6% at 1-sun AM1.5. The limitations to this approach include process complexity, series-resistance effects at high concentrations, and the necessity of Entech coverglass to reduce obscuration losses from increased coverage of metallization in the photo-active area.

The inverted-growth approach [2] to a high-efficiency AlGaAs/GaAs cascade allows the AlGaAs top cell to be grown first at high temperatures. Following the growth of the top cell, the GaAs tunnel interconnect and the bottom cell are grown at lower temperatures. Shown in Fig. 1 is a schematic of the cell structure with a planar GaAs tunnel junction. After the inverted growth, the AlGaAs/GaAs cascade structure is selectively removed from the parent substrate, Ge in this case, for frontside illumination.

We have developed a rapid, multi-wafer, CF_4/O_2 plasma process for selective etching of Ge to produce large-area, thin AlGaAs-GaAs films [3]. The cost of the *sacrificial* Ge substrate is estimated to be comparable to the cost of thin films by other techniques [4,5] where the GaAs substrate must be polished before reuse for further epi growth. Thus, in the process of developing a high efficiency AlGaAs/GaAs cascade using the inverted-growth scheme, we are able to achieve a thin-film AlGaAs/GaAs cascade. This can be advantageously used to develop a current-matched,

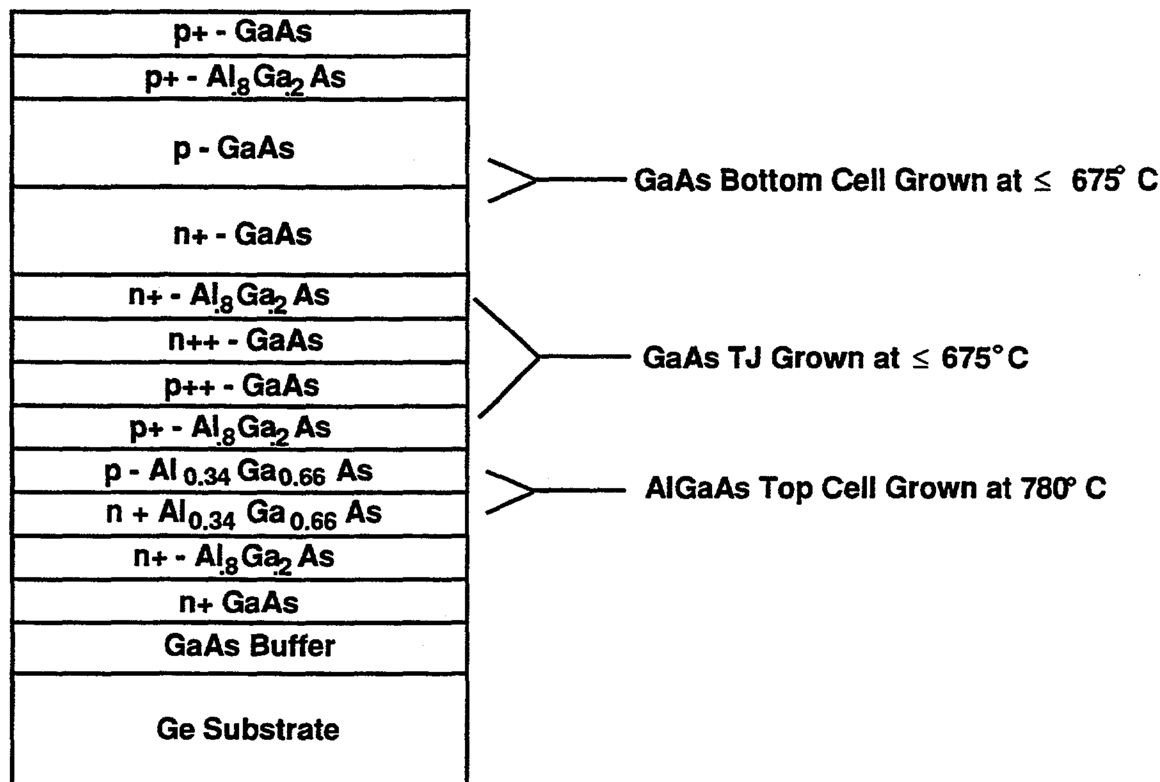

FIGURE 1: Schematic of the inverted-grown AlGaAs/GaAs cascade employing a planar GaAs tunnel junction interconnect.

$Al_{0.37}Ga_{0.63}As$/GaAs/Si (1.90 eV/1.43 eV/1.1 eV bandgap pair), 3-junction cascade shown schematically in Fig. 2. In the schematic, a tunnel-interconnect AlGaAs/GaAs cascade is shown eutectic-metal-bonded (a technique developed in this program) onto an active Si cell. A similar approach can be extended to a 3-junction, $GaInP_2$/GaAs/Si cascade as well.

The development of the high efficiency, inverted-grown, AlGaAs/GaAs cascade cell has focused on the following steps. The Al composition (x) in the top $Al_xGa_{1-x}As$ cell in the cascade was reduced from 0.37 to ~ 0.34 to allow reduction of base-layer thickness of top cell from 3.5 μm to 2.0μm. We have obtained total-area efficiencies of

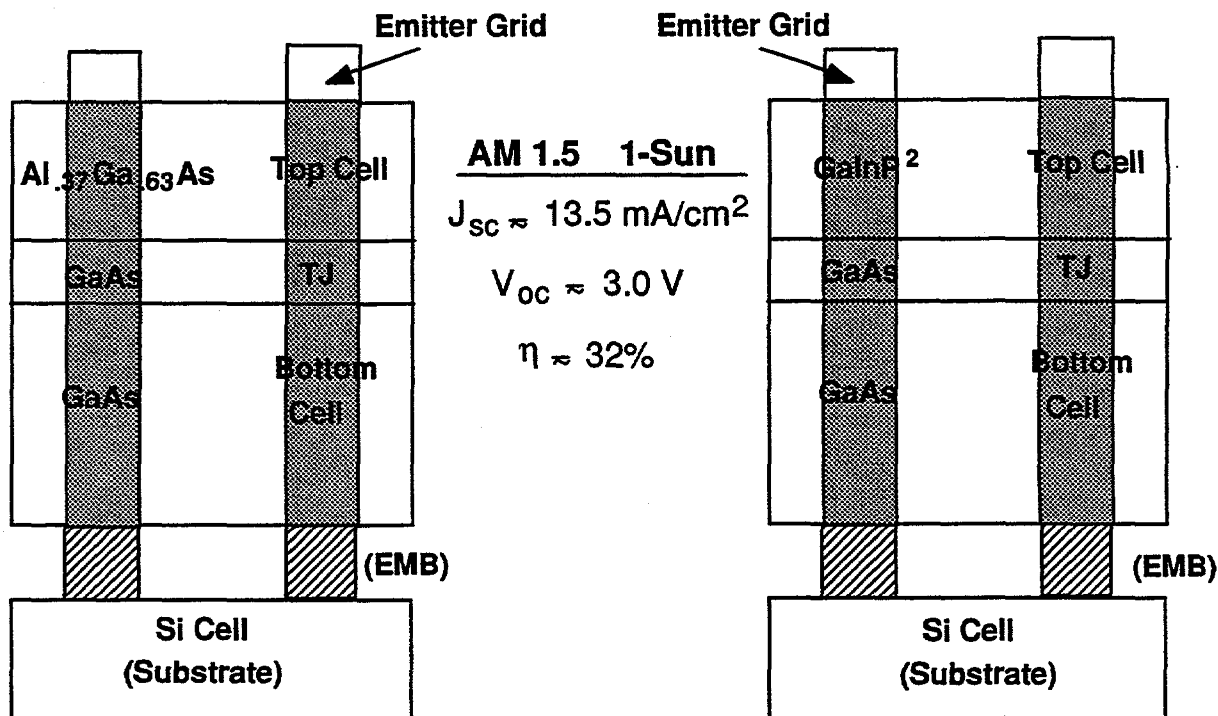

FIGURE 2: Schematic of a current-matched, 3-junction cascade that can be developed using the concept of eutectic metal bonding (EMB) of a monolithic AlGaAs/GaAs cascade or a $GaInP_2$/GaAs cascade to an active Si cell.

13.2% and 15.1% under AM1.5 1-sun and 20-sun concentration, respectively, for such a thin-base $Al_{0.34}Ga_{0.66}As$ (bandgap ~ 1.87 eV) cell. The growth of the GaAs tunnel junction interconnect suitable for inverted-growth of the cascade has been optimized. A technique called eutectic-metal-bonding (EMB) has been developed for strain-free mounting of thin GaAs-AlGaAs films onto a Si carrier substrate. The advantages of EMB compared to bonding of thin-film cells onto glass using commercial adhesives were evident in the photovoltaic performance of thin-film GaAs cells. Thin-film GaAs cells were first developed to evaluate the feasibility of obtaining good photovoltaic characteristics after inverted growth and substrate-removal. A thin film GaAs cell with an active-area efficiency of ~20.3% has been obtained. Then inverted-grown, thin-film, $Al_{0.34}Ga_{0.66}As$/GaAs cascades with an AM1.5 efficiency of 19.9% and 21% at 1- and 7-suns, respectively, has been developed.

3.0 $Al_{0.34}Ga_{0.66}As$ TOP CELL DEVELOPMENT

A key to the development of high efficiency AlGaAs cells for the cascade, is the reduction of moisture and oxygen from source gases and growth ambient [2]. The cell structure optimization also needs to take into account the increase of the near-band-edge absorption coefficients in AlGaAs materials with aluminum content [6]. Hence, the use of thin emitters and attention to preparation of the interface between the n-$Al_{0.34}Ga_{0.66}As$ (bandgap of ~ 1.87 eV) emitter and the n-$Al_{0.85}Ga_{0.15}As$ window can substantially affect cell performance.

Further, an important consideration in the growth of the AlGaAs top cell in the inverted-growth scheme is the ability to preserve the junction characteristic during the thick base layer growth at 780°C. We have observed that the junction characteristics are better preserved during inverted growth if the growth time is limited i.e., a thinner base. Towards this end we have investigated an $Al_{0.34}Ga_{0.66}As$ cell (with only a 2.0 µm base compared to 3.5 µm base in an $Al_{0.37}Ga_{0.63}As$ cell [1]. This cell should be closely current-matched to a GaAs bottom cell under an AM1.5 spectrum. The growth and device optimization of the $Al_{0.34}Ga_{0.66}As$ cell is similar to that for an $Al_{0.37}Ga_{0.63}As$ cell described in Ref. 2. A schematic of the cell structure is shown in Fig. 3. The cell includes a thin $Al_{0.8}Ga_{0.2}As$ window of only ~ 300 Å and an emitter region of ~ 0.15 µm. The spectral responses of two $Al_{0.34}Ga_{0.66}As$ cells with two window layer thicknesses are indicated in Fig. 4, indicating the improved blue response in the range of 440-290 nm with thin window layers. Also observed in the spectral response data is the reduced red response in the AlGaAs cell when the base thickness is reduced.

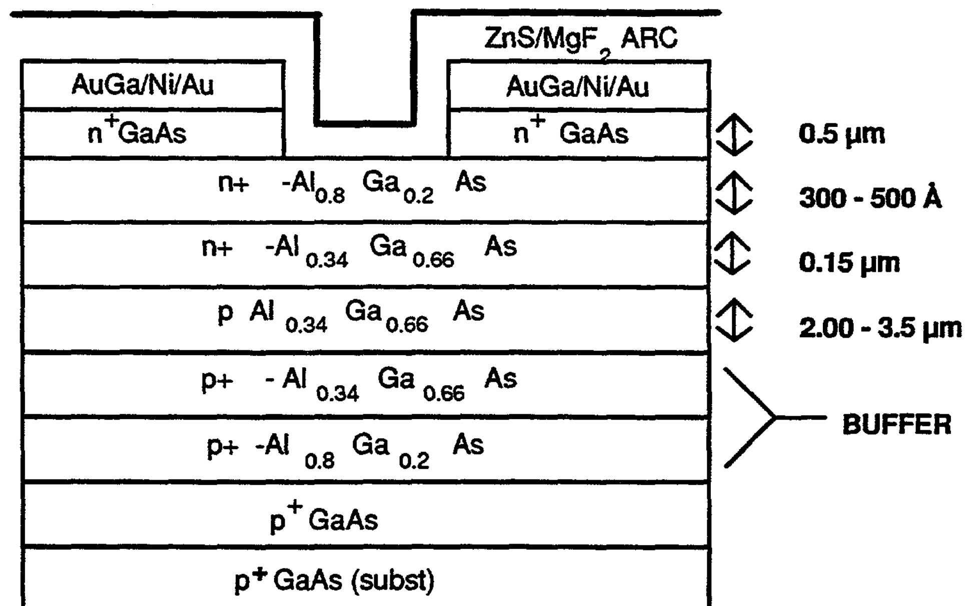

FIGURE 3: Schematic of the $Al_{0.34}Ga_{0.66}As$ top cell being developed for the inverted-grown AlGaAs/GaAs cascade.

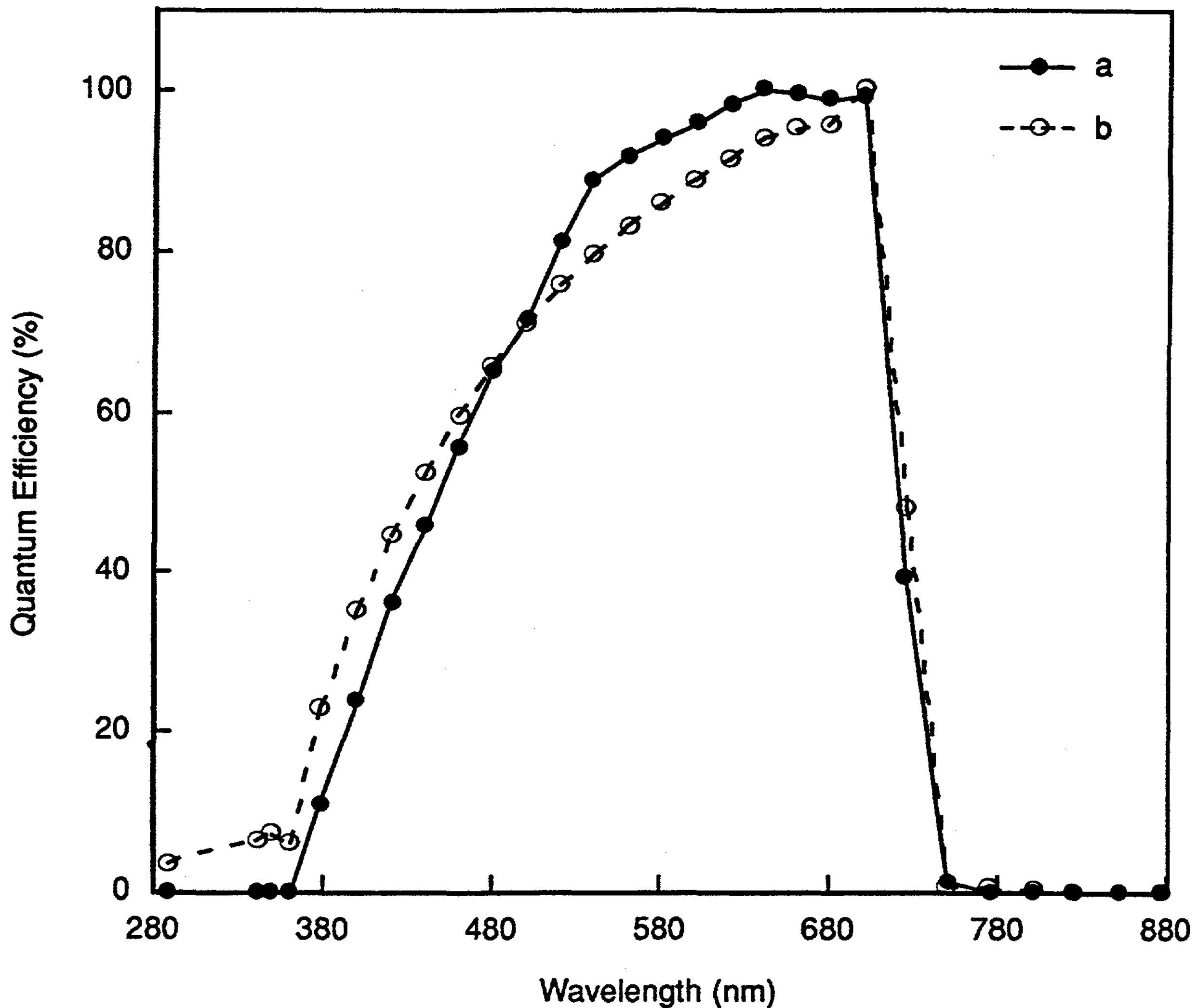

FIGURE 4: Spectral response of $Al_{0.34}Ga_{0.66}As$ (a) cell with a 3.5 μm-base and 500 Å $Al_{0.8}Ga_{0.2}As$ window and (b) cell with a 2 μm-base and 300 Å $Al_{0.8}Ga_{0.2}As$ window.

We also note that the effect of reducing the base layer thickness in the top $Al_{0.34}Ga_{0.66}As$ cell from ~ 3.0 μm to ~ 2.0 μm, compatible with inverted-growth, allows us to obtain an improved open-circuit voltage (up from 1.229V to 1.246 V) and also an improved fill-factor. The I-V data of two such cells are shown in Fig. 5a and 5b. Our best $Al_{0.34}Ga_{0.66}As$ cell has an AM1.5 1-sun total-area efficiency of 13.2% (Fig. 5b). This corresponds to an active-area efficiency of 15.2%. The cell has a 20-sun total-area efficiency of 15.1% and an active-area efficiency of 17.3% (RTI measurement).

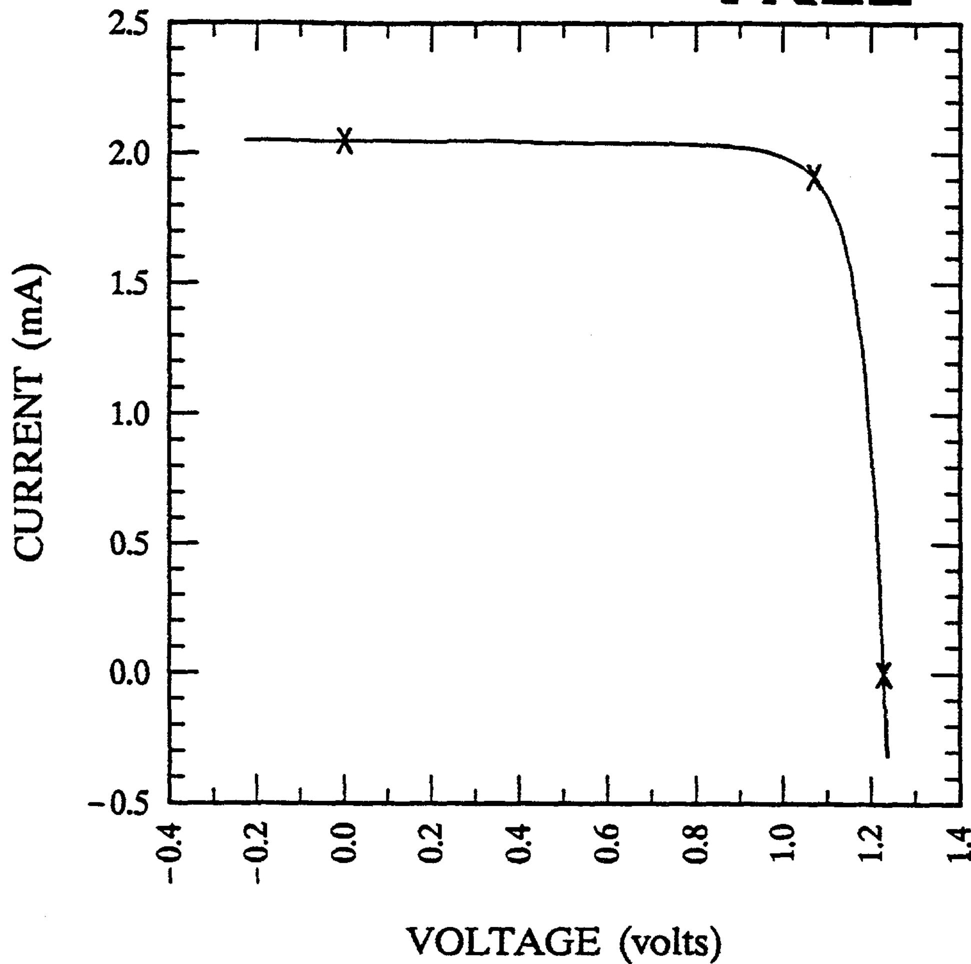

V_{oc} = 1.229 volts	I_{sc} = 2.047 mA
J_{sc} = 11.90 mA/cm²	P_{max} = 2.049 mW
Fill factor = 81.47 %	I_{max} = 1.916 mA
Efficiency = 11.9 %	V_{max} = 1.069 V

FIGURE 5a: I/V data on an $Al_{0.34}Ga_{0.66}As$ cell with a base thickness of 3.5 µm and an $Al_{0.8}Ga_{0.2}As$ window of ~500Å thickness.

RTI AlGaAs/GaAs, direct,1kW/m²

Sample: 1–1479 | Temperature = 25.0°C

Jun. 5, 1992 1:13 pm | Area = 0.173 cm²

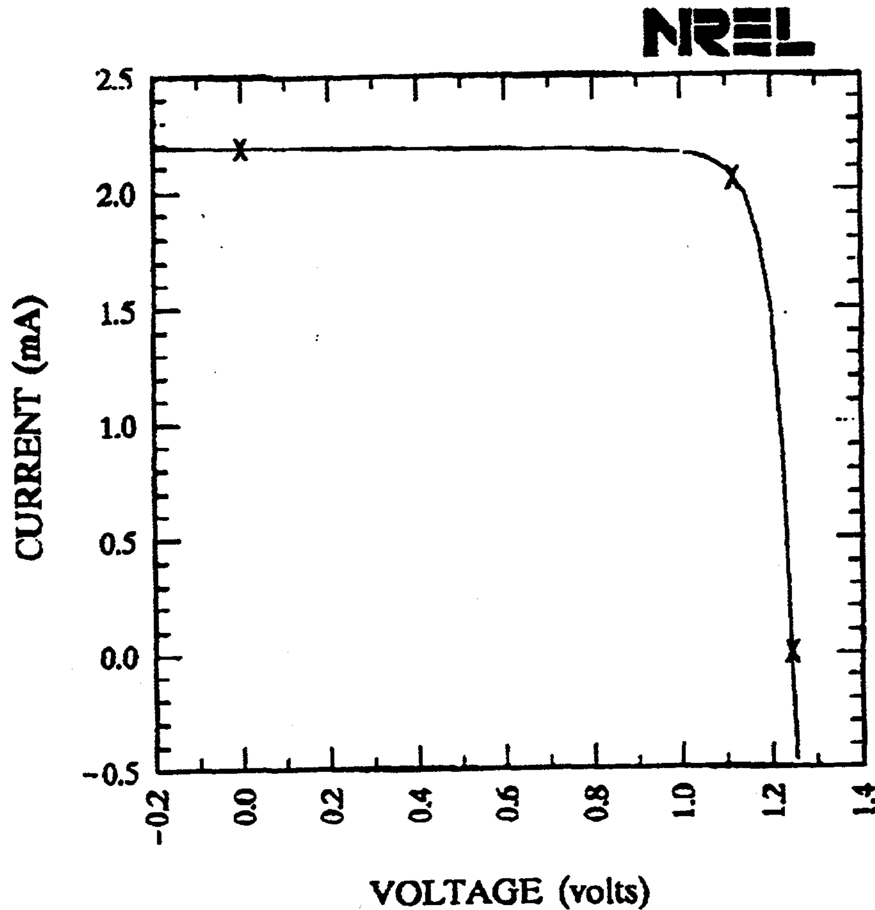

V_{oc} = 1.246 volts | I_{sc} = 2.185 mA

J_{sc} = 12.63 mA/cm² | P_{max} = 2.289 mW

Fill factor = 84.08 % | I_{max} = 2.047 mA

Efficiency = 13.2 % | V_{max} = 1.118 V

FIGURE 5b: I/V data on an $Al_{0.34}Ga_{0.66}As$ cell with a base thickness of ~ 2.0 µm and a window layer of 300 Å, compatible with the inverted growth of the cell at 780°C.

4.0 GaAs TUNNEL JUNCTIONS FOR INVERTED-GROWN CASCADES

Development of high-conductance GaAs tunnel interconnects for the AlGaAs/GaAs cascade (shown in Fig. 1) is necessary to reduce ohmic losses. GaAs p^{++} - n^{++} tunnel junctions have been grown using zinc as the dopant for the p^{++}- regions and Se as the dopant for the n^{++} -regions. The tunnel junctions were grown at 650 to 675°C.

A schematic cross section of a typical tunnel junction with various layer thicknesses is shown in Figure 6. The tunnel diode area is 9×10^{-4} cm^2. The specific contact resistance of the AuGe/Ni/Au (500Å/150Å/2000Å) multilayer metallization to the n^+- GaAs substrate, sintered at 350°C for 30 s, was measured to be less than 1×10^{-4} ohm - cm^2. This specific contact resistance is about a factor of thirty lower than the lowest specific contact resistance obtained for the best GaAs tunnel junction in this work. The specific resistivity of non-sintered Ti/Au (500Å/2000Å) metallization to p^+ - GaAs was measured to be 6×10^{-6} ohm - cm^2. The contact resistivities of ohmic metallizations were obtained from transmission line model (TLM) patterns [7].

The use of *cycled growth* for improved conductance of GaAs tunnel junctions was mentioned in our last annual report. The characteristics of GaAs tunnel diodes with continuous growth for GaAs:Se and either continuous or cycled growth for GaAs:Zn are shown in Fig. 7a and 7b, respectively. The peak current density (J_p) of the tunnel junction with the cycled GaAs:Zn is larger by a factor of about 65 and the specific resistance is correspondingly smaller by the same amount than that of the junction with continuously grown GaAs:Zn. The increase in conductance (Fig. 7b) is also accompanied by the disappearance of a well-marked negative differential resistance (NDR) (in Fig. 7a). By plotting the J_p values versus effective doping concentration (as discussed in Ref. 8) for both cases, we find that J_p in Fig. 7a is smaller than the theoretical value by a factor of two, while the J_p in Fig. 7b is higher than the theoretical value by about two orders of magnitude.

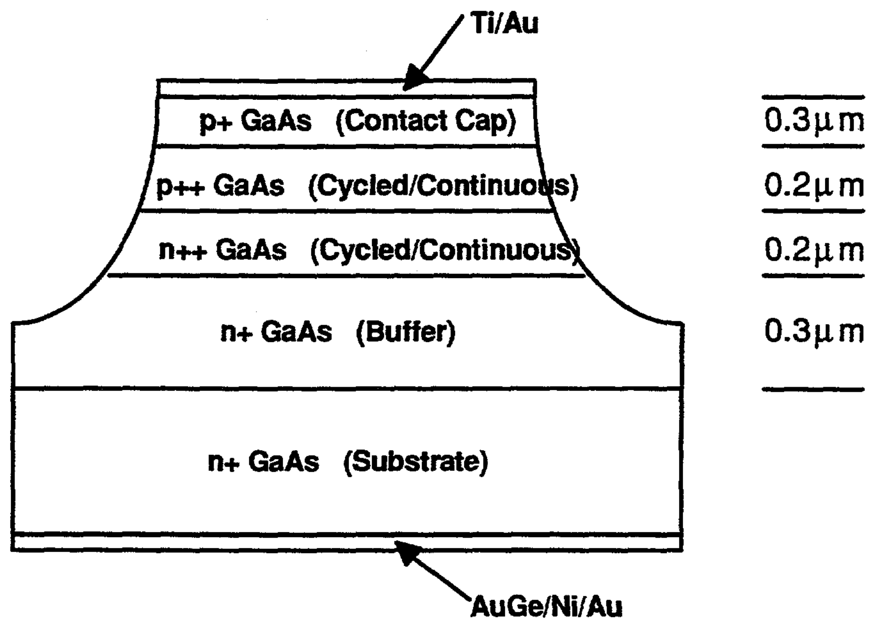

FIGURE 6: Schematic of a typical GaAs tunnel junction with the various layer specifications, used to evaluate the use of cycled growth.

H:0.5V/div. V:20 μA/div.

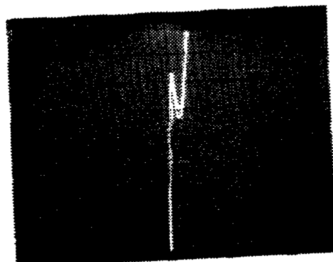

(a)

H:0.1V/div. V:2 mA/div.

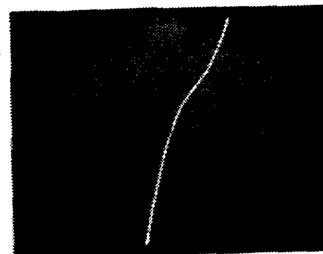

(b)

H:0.5V/div. V:20 μA/div.

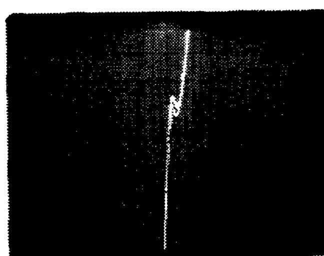

(c)

FIGURE 7: I/V characteristics of GaAs tunnel junctions grown with continuous growth for GaAs:Se, and (a) continuous and (b) cycled growth for GaAs:Zn. Shown in (c) is the I/V characteristic for a tunnel junction with cycled growth for GaAs:Se and GaAs:Zn.

We note that the GaAs tunnel junction grown with both cycled GaAs:Zn and GaAs:Se regions has the NDR (Fig. 7c) and a J_p value consistent with the theoretical value based on doping levels.

Similar improvements in J_p and the conductance of the tunnel junctions with cycled GaAs:Zn regions were observed at a growth temperature of 650°C (Table 1). However, the factor of improvement in J_p was ~ 50 compared to ~ 65 seen at a growth temperature of 700°C. At a growth temperature of 650°C, we have obtained a J_p of 12.8 A / cm^2 and a specific contact resistance of 3.3×10^{-3} ohm - cm^2. This is comparable to the smallest reported value of 3.0×10^{-3} ohm - cm^2 for a GaAs tunnel junction grown at 520 °C, by molecular beam epitaxy [9].

Using a cycled GaAs:Zn layer in a GaAs tunnel junction with Si as the dopant for the n^+- region leads to a reduction in J_p and, correspondingly, the specific-resistance, mainly as a result of the decrease in hole concentration in the cycled GaAs:Zn. The I-V characteristics of tunnel junctions with GaAs:Si for the n^+- regions using continuous growth and cycled growth for GaAs:Zn are indicated in Fig. 8a and 8b, respectively. The NDR is pronounced in both I-V characteristics; this contrasts with those shown in Fig. 7a and 7b. It has also been observed that the J_p values were within about 20-30 percent of the theoretical values for the respective doping levels when Si-doping is used. The cycled growth of GaAs:Si did not affect the J_p and the conductance values regardless of whether a cycled or continuous GaAs:Zn layer was used to make the tunnel junction.

We can explain the tunnel junction results in terms of the *cycled* growth material properties, discussed in **Appendix 1.** In the case of tunnel diodes with GaAs:Se (continuous) and GaAs:Zn (cycled) doping, the presence of V_{Ga} - Se_{As} defects in the n^+ GaAs region and Zn_i in the p^+ GaAs region assist in extra carrier tunneling. Thus, J_p is about two orders of magnitude higher than the theoretical value, and the NDR disappears

1:0.5V/div. V:20 μA/div.

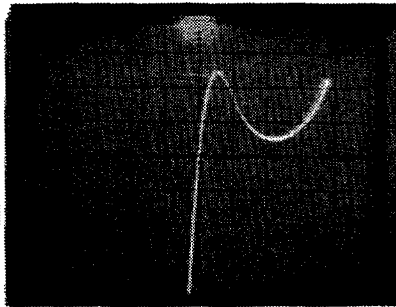

(a)

H:0.5V/div. V:20 μA/div.

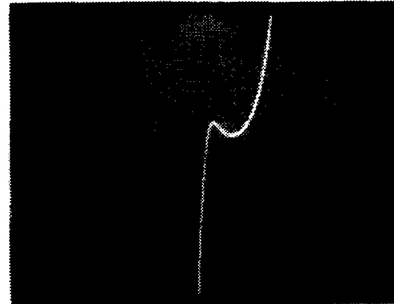

(b)

FIGURE 8: I/V characteristics of tunnel junctions with GaAs:Si for the n^+- regions and (a) continuous growth and (b) cycled growth for GaAs:Zn.

as a result of this excess current. However, with a cycled GaAs:Se layer for n^+ GaAs, the concentration of V_{Ga} - Se_{As} centers are probably low due to thermal annealing. Thus, even though Zn_i defects are likely in the p^+ GaAs side of the tunnel junction, there are probably no accompanying states in the n^+ GaAs to complete the carrier tunneling. Thus, the GaAs tunnel junction with cycled GaAs:Se and GaAs:Zn layers show NDR as well as a J_p close to the theoretical value for the doping level.

In the case of a GaAs:Si and GaAs:Zn system, the low levels of Si_{Ga} - V_{Ga} complexes in GaAs:Si probably limit extra carrier tunneling even though Zn_i defects are present in the cycled GaAs:Zn region. Hence, we obtain near ideal J_p values which are consistent with the doping levels under all conditions of growth of GaAs tunnel junctions with Si doping for the n^+ GaAs region.

TABLE 1: Peak tunnel current density of GaAs tunnel junctions at different growth temperatures using continuous and cycled growths for GaAs:Zn.

Growth Temperature (°C)	J_p of Tunnel Diode (mA/cm^2) GaAs:Se Continuous	
	Zn: Continuous	Zn: Cycled
700	47	3000
650	256	12800*

* Specific resistance of 3.3×10^{-3} ohm - cm^2

In the inverted-grown cascade cell results obtained in this study, tunnel-junction conductance deteriorates if the GaAs bottom cell is grown at > 675°C. Also, the use of $Al_{0.8}Ga_{0.2}As$ hetero-barriers on either side of the GaAs tunnel junction, as shown in Fig. 9, improve thermal stability of the GaAs tunnel junction during the GaAs cell growth. The beneficial effects of these hetero-barriers on tunnel junction conductance have been noted earlier [10].

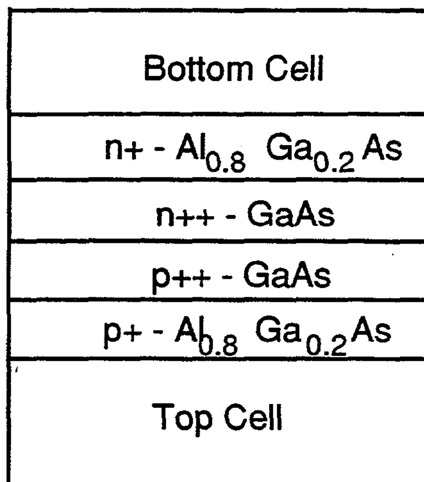

FIGURE 9: Schematic of a GaAs tunnel junction including the $Al_{0.8}Ga_{0.2}As$ hetero-barriers for improved thermal stability during the inverted growth of the GaAs bottom cell.

5.0 EUTECTIC METAL BONDING

After the inverted growth of the $Al_{0.34}Ga_{0.66}As$/GaAs cascade, the removal of the parent-substrate for front-side illumination (see Fig. 1) requires the bonding of the thin-film cascade onto a carrier substrate. Ideally, the AlGaAs-GaAs thin films should be bonded onto these carrier substrates with little stress since stress can interfere with subsequent cell processing. We have been able to obtain photovoltaic-device-quality GaAs-AlGaAs thin films bonded onto Si substrates using an approach denoted as eutectic-metal-bonding (EMB).

EMB involves the growth of GaAs-AlGaAs films (device structures) on lattice-matched Ge substrates. The steps involved in the uniform, reproducible growth of GaAs-AlGaAs structures on Ge have been discussed elsewhere [11]. Following the epitaxy, a film of gold is evaporated onto the face of the epitaxial structure and a clean Si substrate. The Si substrate is given a rinse in 1:100 HF solution and blown dry prior to evaporation. The two Au-coated samples are stacked face-to-face in an alloying furnace, placed in intimate physical contact, and bonded at ~ 400°C. The bonding of the GaAs-AlGaAs structure to the Si substrate occurs by the formation of low-temperature eutectics of Au-Si and Au-GaAs[12]. The phase diagrams of the Au-Si and Au-Ga-As systems, showing their respective eutectics, are indicated in Fig. 10a and 10b [13]. The schematic for obtaining the thin EMB GaAs-AlGaAs films on Si is indicated in Fig. 11. The advantages of using a buffer (shown in Fig. 11) are discussed further below.

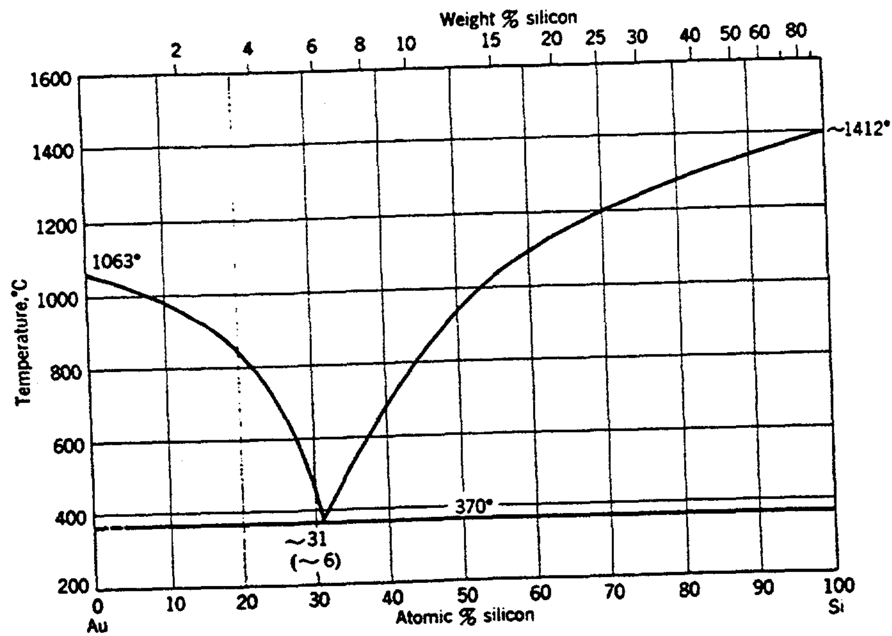

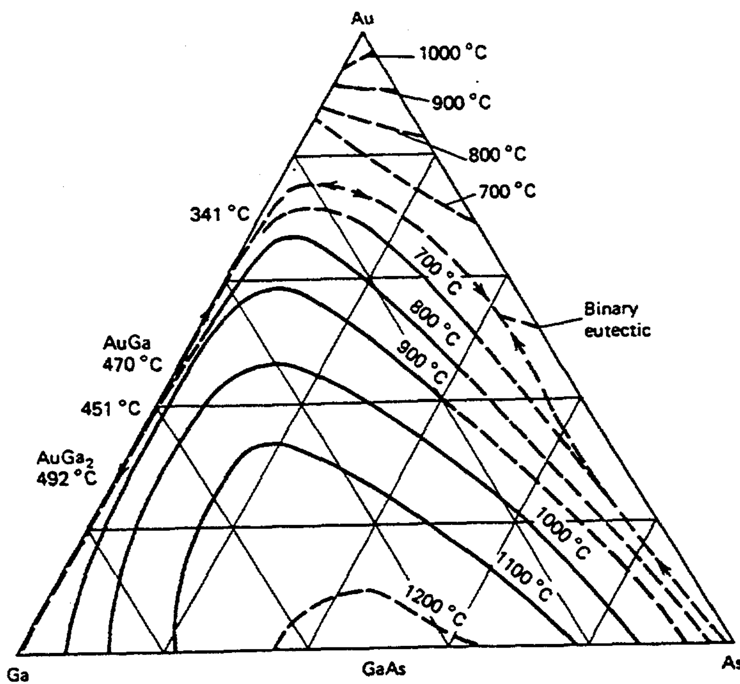

FIGURE 10: Phase diagrams of the a) Au-Si and b) Au-Ga-As systems, indicating the formation of the Si-Au eutectic and a range of AuGa eutectics at ~400°C (from Ref. 13).

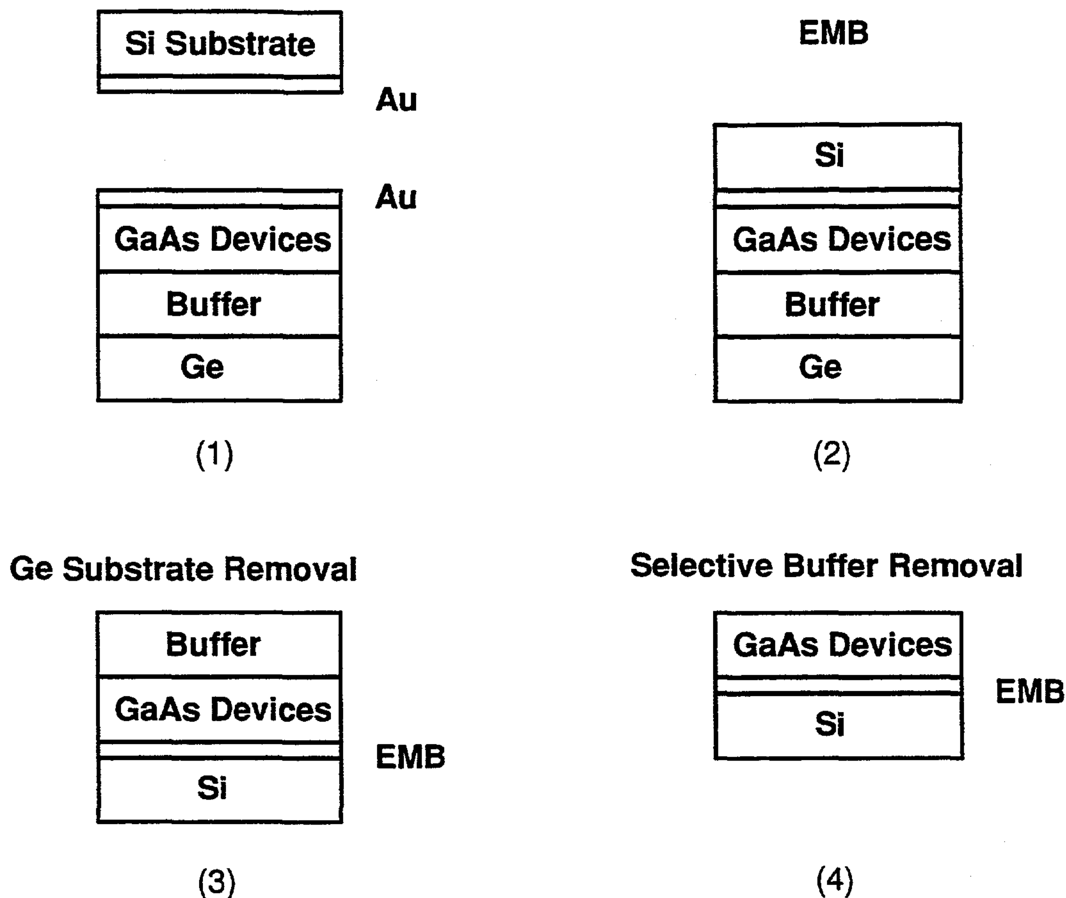

FIGURE 11: Schematic of the steps to produce EMB AlGaAs/GaAs thin films on Si.

In contrast to the bonding by atomic rearrangement (BAR) technique [14] developed recently for InP-based materials on GaAs, the EMB approach is a low-temperature process and, more importantly, does not involve precise crystallographic alignment of Si and GaAs. Rather, we have been able to obtain EMB between Si and GaAs for any arbitrary alignment of the two respective crystal orientations. Following the EMB of GaAs-AlGaAs structures on Si, the Ge substrate is selectively removed by a CF_4/O_2 plasma etch. This etch does not attack GaAs or AlGaAs, and leaves excellent surface-quality GaAs-AlGaAs films. The details of this etching process have been described elsewhere [3].

Aspects of long-range order and residual elastic strain in the EMB GaAs/AlGaAs thin films on Si substrates were studied by Raman spectroscopy. Shown in Fig. 12 is the Raman spectrum obtained from a GaAs layer at 300K using an Ar^+ ion laser (514.5 nm

excitation). First-order scattering from the longitudinal optical (LO) phonon at 291.8 cm^{-1} and transverse optical (TO) phonon at 268.8 cm^{-1} are clearly observed. Also apparent are scattering from second-order transverse acoustic (2TA) phonons in the 120-200 cm^{-1} range and the TO+TA combination band at 334 cm^{-1}. The determination of strain indicates that the residual elastic strain in the EMB GaAs-AlGaAs samples is substantially lower (by a factor of 9) compared to heteroepitaxial GaAs films deposited directly on Si(100) substrates [15].

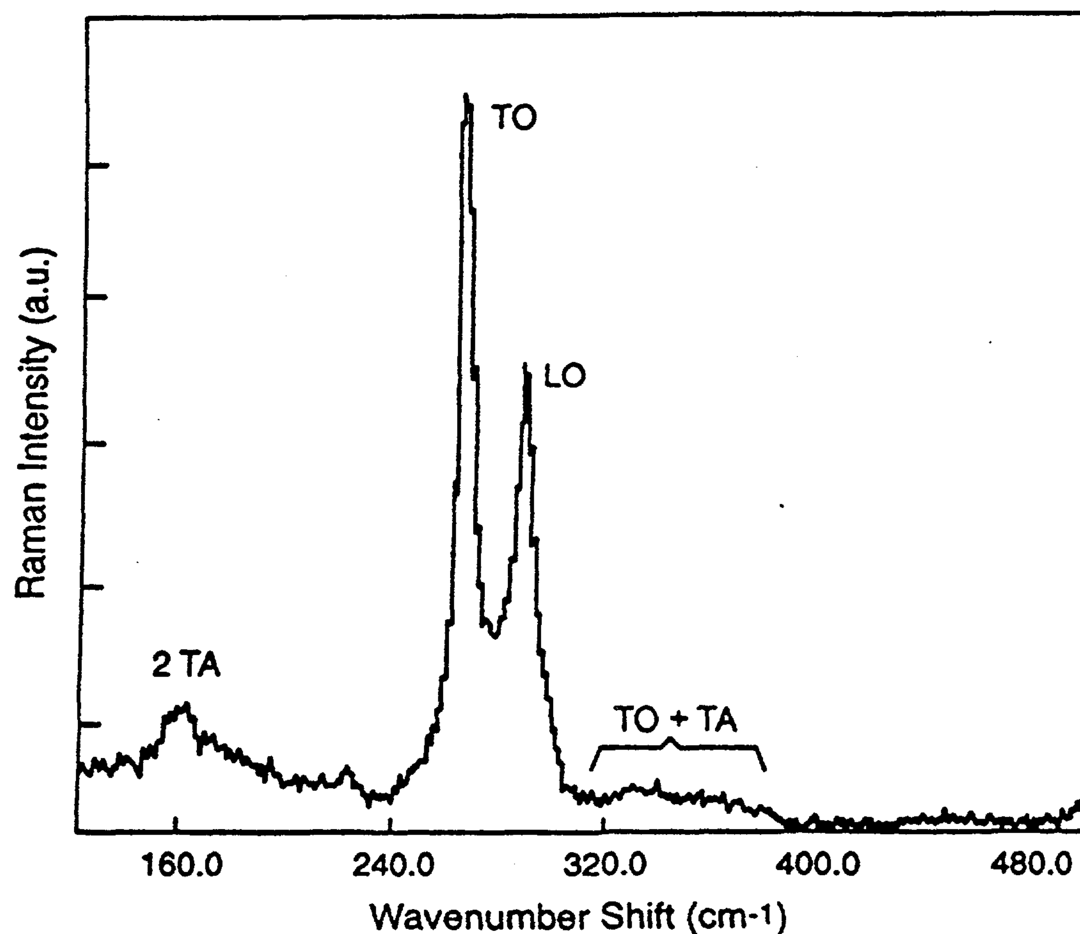

FIGURE 12: Raman Spectrum from an EMB GaAs thin film on Si, obtained using an Ar^+ ion laser excitation at 514.5 nm.

The quality of the EMB GaAs films on Si substrates can be significantly affected by the Ge autodoping, especially since the GaAs material that is available for device-fabrication is the one that was originally closer to the Ge substrate. The autodoping

problem can be avoided by the use of ~ 3.5 μm-thick GaAs buffers. These GaAs buffers can be selectively removed later using AlGaAs etch-stop layers [16].

The 300K PL from a 3.5-μm-thick GaAs buffer and from a GaAs layer (in a double heterojunction with $Al_{0.8}Ga_{0.2}As$ windows) grown after the buffer, are indicated in Fig. 13. In both cases, the PL is measured using identical excitation and detection conditions. The DH structure was bonded to Si using EMB. The band edge PL intensity of the GaAs layer grown after the buffer is over 250 times more intense than that of the buffer. Also, the 300K PL full-width at half-maximum of this GaAs layer is ~ 29 meV. The pronounced oscillations for the sub-bandgap PL (Fig. 13a) and a weak oscillation in the band-edge PL (Fig. 13b) due to Fabry-Perot action (multiple-beam interference in a cavity-like structure) can be observed. The Fabry-Perot action attests to the smoothness of the AlGaAs-GaAs films grown on Ge, and after the removal of the Ge substrate following EMB onto Si [12].

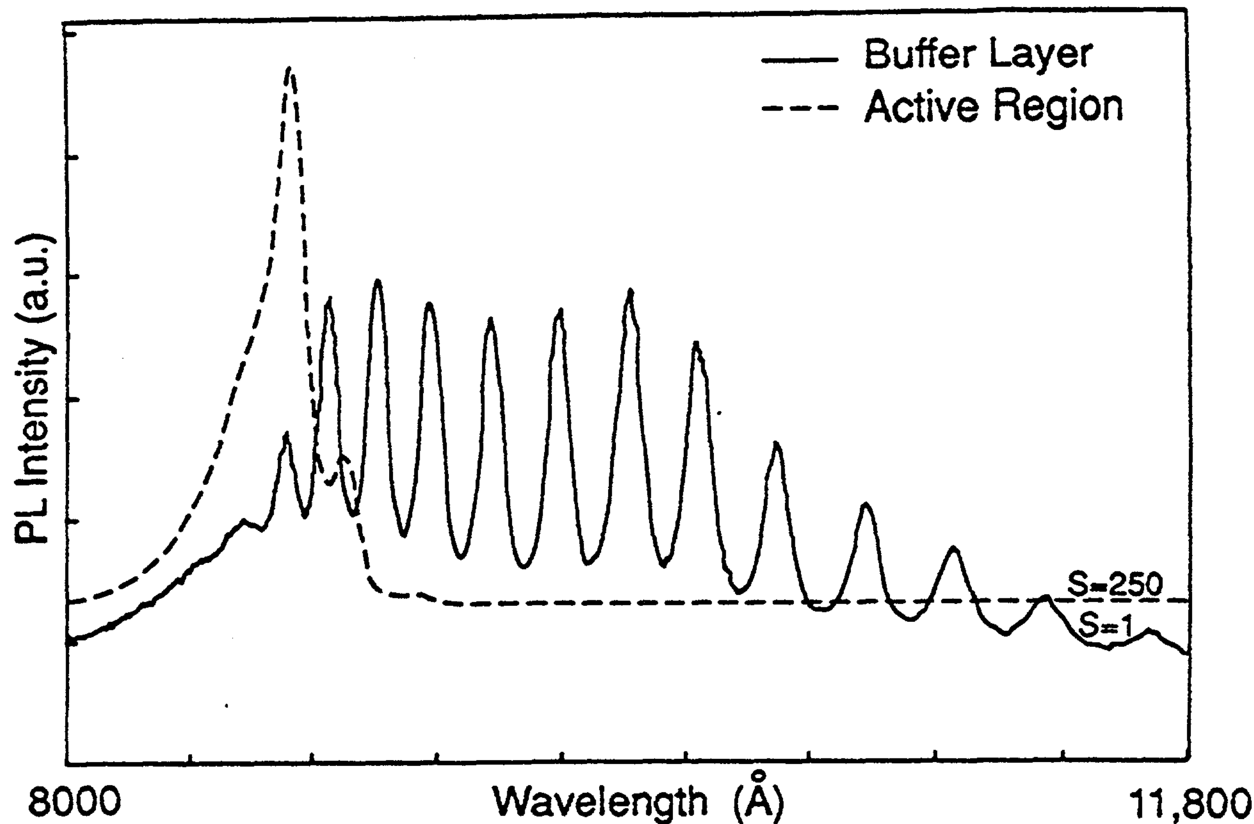

FIGURE 13: 300 K PL spectra from an EMB GaAs thin film obtained from (a) the GaAs buffer originally adjacent to the Ge substrate, (b) the GaAs active layer after the selective removal of the GaAs buffer. S is the lock-in-amplifier sensitivity i.e., lower sensitivity implies larger signal.

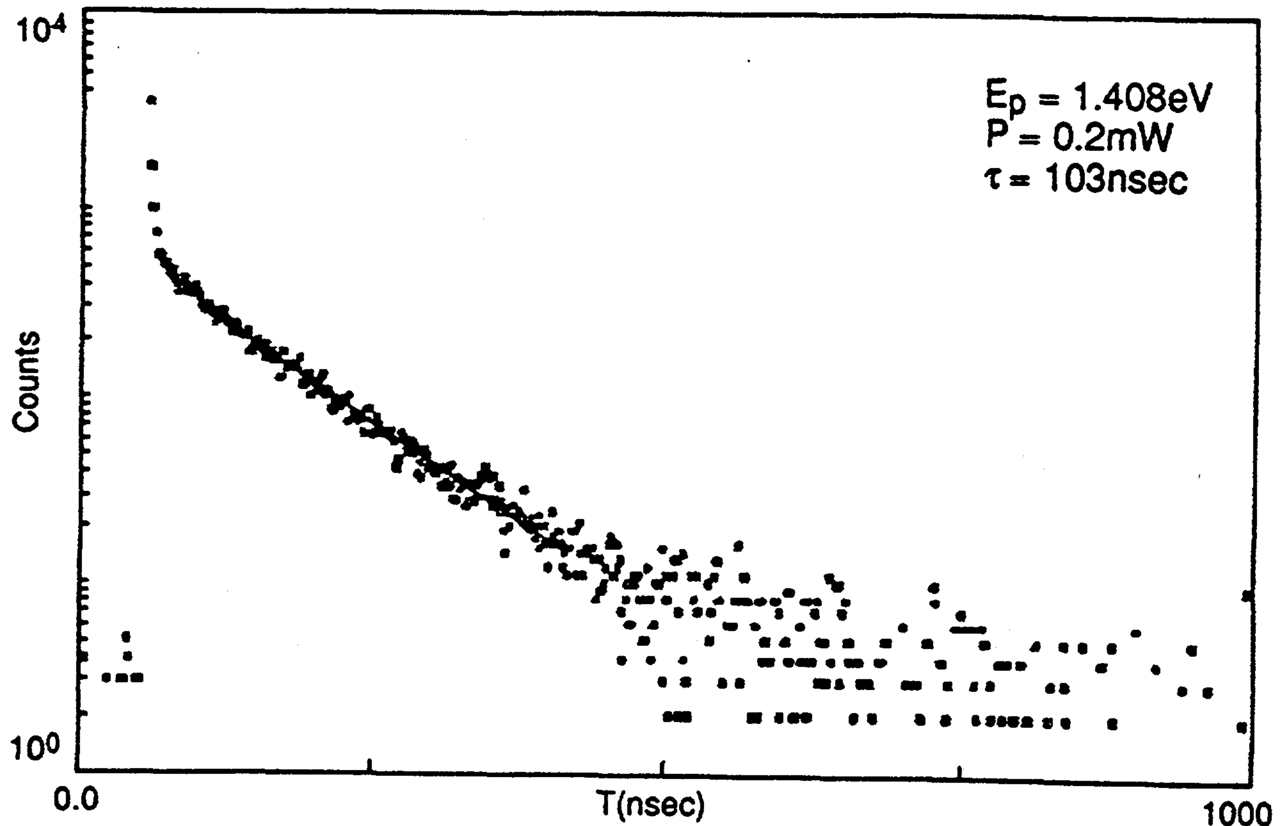

Figure 14: 300K PL decay from an EMB GaAs/AlGaAs DH structure on Si.

The high quality of the EMB GaAs thin films using a buffer to control Ge auto-doping followed by subsequent removal of the buffer, is evident in the PL decay lifetime data from a GaAs DH structure. Shown in Fig. 14 is the PL transient observed in such an EMB GaAs-AlGaAs DH structure. The PL decay is a single exponential over two decades with a lifetime of 103 nsec. The measured lifetime at a laser power of 2.0 mW was ~ 99 nsec. The similarity of these two values indicates that the material quality is excellent, and traps and deep level defects play a negligible role in recombination dynamics. The lifetime of 103 nsec is about forty times larger than the state-of-the-art minority-carrier lifetime for a heteroepitaxial GaAs film on Si [17]. Also, this lifetime is about three times the reported lifetime of ~ 32 nsec obtained from a freestanding GaAs thin film prepared by the cleavage of lateral epitaxial films for transfer (CLEFT) process [5].

6.0 INVERTED-GROWN GaAs THIN FILM SOLAR CELLS

The feasibility of inverted-growth on a *sacrificial* Ge substrate and the associated cell emitter-grid processing in EMB GaAs-AlGaAs thin films on Si (after Ge substrate removal) are indicated by our results on thin-film GaAs solar cells. Several thin-film GaAs solar cells, grown under identical conditions, have been bonded to Si, using EMB and to glass using a commercial adhesive (DC 93-500). The cells bonded to Si show improved open-circuit voltages (V_{oc}) and fill-factors (FF). The Au-coating (for EMB) on the backside of the thin-film cell is a good reflector [12] for utilizing possible photon-recycling effects. This was evident in the excellent J_{sc} values in the GaAs thin film cells. Also, the use of a 3.5-μm-thick GaAs buffer to reduce Ge autodoping was found to improve the V_{oc} and FF. The best EMB, thin-film GaAs cell on Si has a V_{oc} of 0.96 V, a J_{sc} of 27.8 mA/cm^2, a FF of 0.76, and a total-area efficiency of 20.3% under AM1.5D. We believe that the efficiency is limited by series resistance associated with the use of non-alloyed AuGe/Ni/Au contact to the emitter as well as the point-contacting of the back-contact during measurement, causing the fill-factor to be lower than in a conventional GaAs cell. The emitter contacts are not sintered because of the thin film structure.

The I-V data measured at NREL on an EMB thin-film GaAs cell on Si are shown in Fig. 15 and indicates an efficiency of 14.0%. Based on RTI measurements, the active-area efficiency of this cell is ~ 17.9%. The spectral-response data measured at NREL for the same cell are shown in Fig. 16. The near-flat spectral-response (≥90%) in the spectral-range of 700-850 nm indicates excellent diffusion length in the EMB GaAs thin films. The measured internal quantum efficiency at 801 nm is ~ 0.9376. This value can be used to estimate the diffusion length in the EMB GaAs films, and compared with an estimate from a minority-carrier lifetime of ~100 ns (discussed earlier), as follows. The photogenerated current in a (n^+-p) solar cell can be approximated [18] under monochromatic illumination (especially for wavelengths very

RTI Thin Film GaAs, direct,1kW/m²

Sample: 1−1454 Temperature = 25.0°C

Jun. 5, 1992 12:32 pm Area = 0.174 cm²

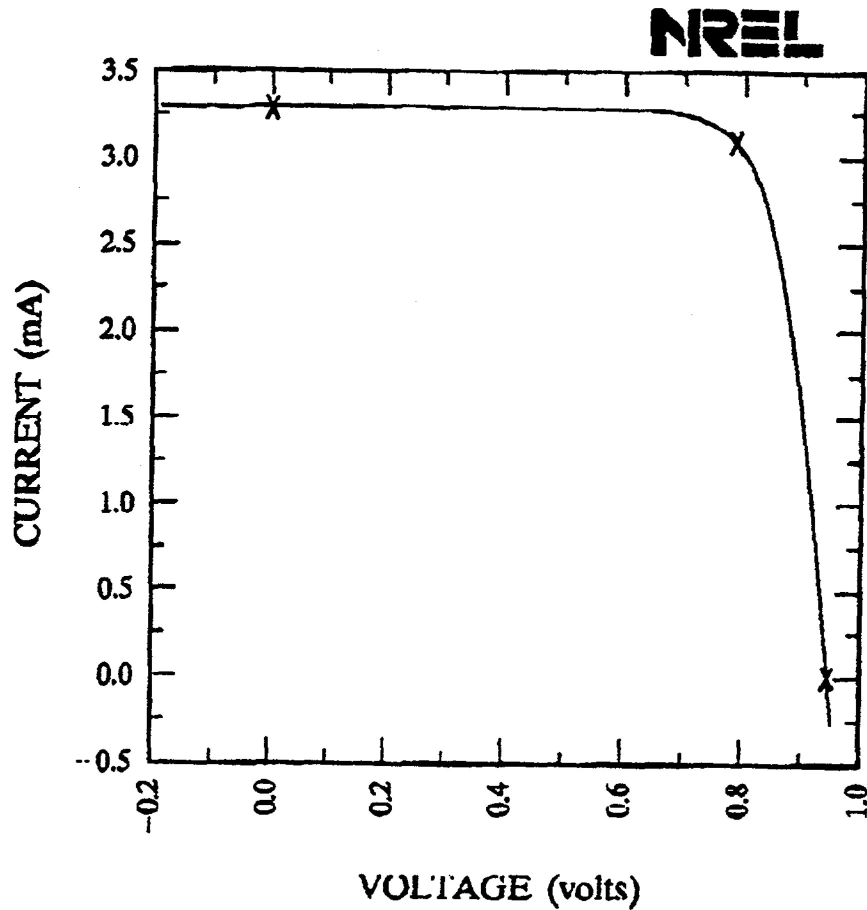

V_{oc} = 0.9455 volts I_{sc} = 3.287 mA

J_{sc} = 18.89 mA/cm² P_{max} = 2.432 mW

Fill factor = 78.25 % I_{max} = 3.093 mA

Efficiency = 14.0 % V_{max} = 0.7863 V

Active-Area Efficiency = 17.9% (RTI measurements)

FIGURE 15: I/V data of an EMB thin-film GaAs solar cell on Si.

RTI GaAs Thin Film Eutectic Metal Bonded

Sample: 1-1454 Temperature = 25.0°C

Jun. 3, 1992 3:34 pm Area used = 0.174 cm^2

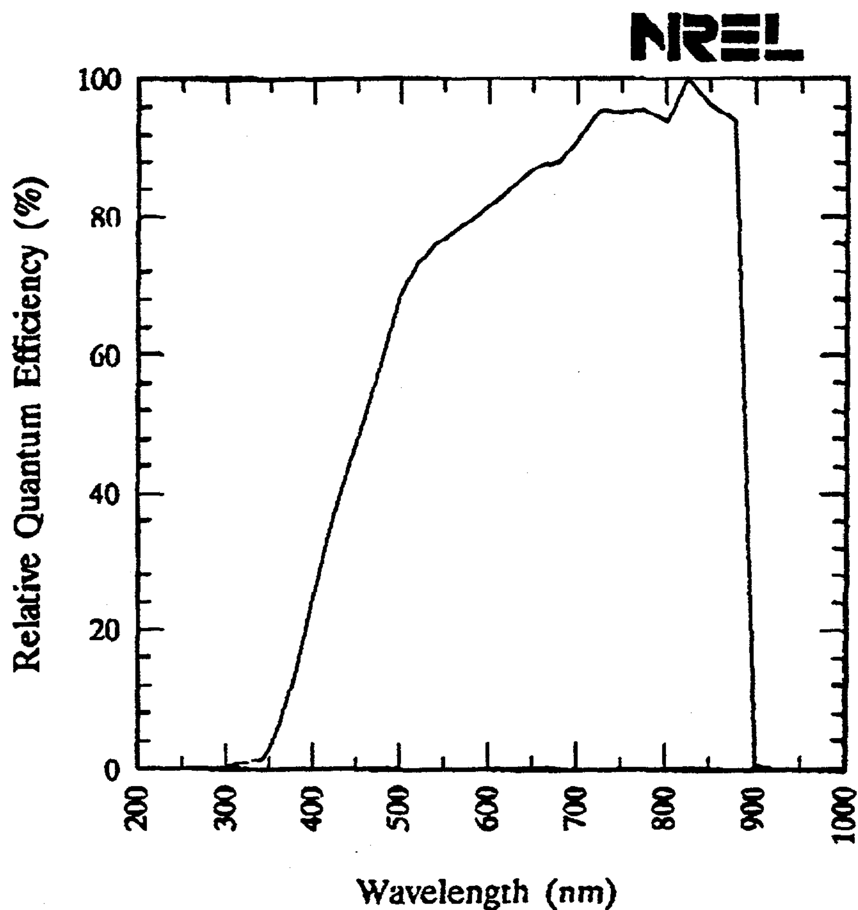

Light bias = 1.00 mA

Zero voltage bias

FIGURE 16 Spectral-response data on an EMB thin-film GaAs solar cell on Si.

close to the band edge and for a thin emitter cell), as

$$J_n(\lambda) = q\,N(\lambda)(1-R(\lambda))\left[1-\exp(\alpha W)+\frac{\alpha(\lambda)L_n}{\alpha^2 L_n^{\,2}-1}\{(\alpha L_n-1)\exp(-\alpha W)+\beta\}\right]$$

where β is given by

$$\beta = \frac{2\left[\exp(-\alpha L)-\exp(-\alpha W)\exp\left(\frac{W-L}{L_n}\right)\right]}{\exp\left(\frac{L-W}{L_n}\right)-\exp\left(\frac{W-L}{L_n}\right)}$$

and N(λ) is the incident photon flux, R(λ) is the reflectance of the surface, α(λ) is the absorption coefficient in the semiconductor, W is the width of the depletion layer in the p-base, L_n is the electron diffusion length in the p-base, q is the electronic charge, and L is the thickness of the base. The internal quantum efficiency at a wavelength λ, I(λ), can be written as

$$I(\lambda) = \left[1-\exp(\alpha W)+\frac{\alpha(\lambda)L_n}{\alpha^2 L_n^{\,2}-1}\{(\alpha L_n-1)\exp(-\alpha W)+\beta\}\right]$$

For a nominal base doping level of ~ 4 x 10^{17} cm^{-3} and under short-circuit spectral-response conditions, we obtain a depletion layer width of 0.03 μm. At a wavelength of 801 nm, we can assume the absorption coefficient α(λ)) as 2.0 x 10^4 cm^{-1} [19] in GaAs. The thickness of the base of the cell is ~ 4.0 μm. Under these conditions, the expression for β reduces to

$$\beta = \frac{2\left[\exp(-\alpha L) - 1\right]}{\exp\left(\frac{2L}{L_n}\right) - 1}$$

and the internal quantum efficiency can be written as

$$I(\lambda) = \left[1 + \frac{2}{\alpha L_n}\left[\frac{\exp(-\alpha L) - 1}{\exp\left(\frac{2L}{L_n}\right) - 1}\right]\right]$$

Substituting the measured value of internal quantum efficiency as 0.9388 and other device parameters, we can iteratively solve for the electron diffusion length in the p-base. We obtain a diffusion length of ~ 7.0 μm ± 2.0 μm. This value is reasonable considering an estimated diffusion length of ~ 16 μm based on the measured lifetime of ~ 100 ns (in the EMB GaAs thin film at a doping level of ~ 1×10^{17} cm^{-3}) and a minority-carrier (electron) mobility of 1000 cm^2/Vsec at these doping levels [19].

7.0 THIN-FILM $Al_{0.34}Ga_{0.66}As$/GaAs CASCADES

Thin-film, inverted-grown, $Al_{0.34}Ga_{0.66}As$/GaAs cascade results reported in this section, were grown on GaAs substrates (and subsequently removed) since the growth of high-efficiency $Al_{0.34}Ga_{0.66}As$ cells and the cascades on Ge substrates were not optimized. The cascade results reported here are for thin-films bonded to glass support substrates. Cascade results based on EMB-Si structures need to be developed as well and are likely to offer the advantages noted in the previous section for thin-film GaAs cells.

The I-V data on our best $Al_{0.34}Ga_{0.66}As$/GaAs cascade is shown in Fig. 17. The cell has a V_{oc} of 2.06 V, smaller by about 0.2 V from the expected value, probably a result of increased dark-current from the GaAs bottom cell. The short-circuit current density (J_{sc}) of the cascade is ~ 13.3 mA/cm^2 and I-V data suggests the two junctions are apparently current-matched. The fill-factor is 0.73, a relatively low value, caused by the extra shunting in the bottom cell and additional series resistance associated with non-alloyed emitter-contact metallization. The active-area efficiency of the cell at AM1.5 1-sun is ~ 19.9% (RTI measurement), very close to 20.2%, the best reported [10] efficiency for a tunnel-interconnect AlGaAs/GaAs cascade grown by MBE. The effect of even minor solar concentration apparently improves the cascade performance, as shown in Table. 2. The active-area efficiency is ~ 21% at 5-7 AM1.5 suns, at a cell temperature of ~ 65°C. The significant increase in cell temperature to 65°C is attributed to bonding the thin-film cascade structure to glass, (a poor thermal conductor). We believe that EMB onto Si should help to dissipate heat in thin-film cells for concentrator applications. We believe that, with some optimization of growth and device structures, we can realistically achieve an efficiency of ~ 26-27% in these thin-film, inverted-grown, AlGaAs/GaAs cascades at ~ 100 AM1.5 suns.

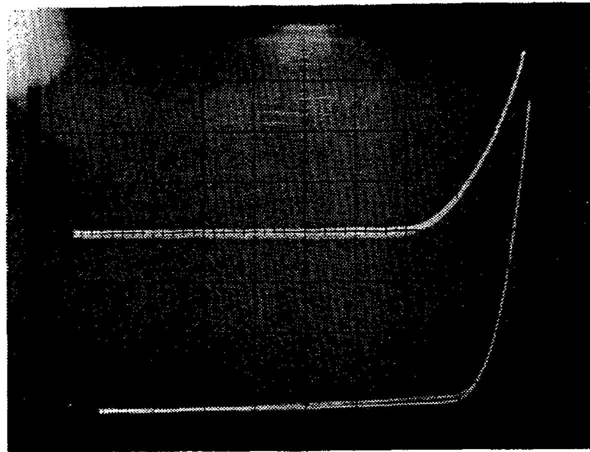

V_{oc} = 2.06V
J_{sc} = 13.3 mA/cm^2
FF = 0.73
η = 19.9%

FIGURE 17: I-V characteristic of a thin-film, inverted-grown, $Al_{0.34}Ga_{0.66}As/GaAs$ cascade under AMI-5D spectrum.

Conc.	V_{oc} (V)	FF	η (%)	Cell Temp
1	2.06	0.73	19.9	25°C
2	2.14	0.74	**21.0**	—
7.7	2.15	0.73	**20.8**	—
25	2.14	0.68	19.3	65 °C

TABLE 2: Effect of solar concentration on cascade parameters.

8.0 SUMMARY AND CONCLUSIONS

In summary, we have provided the first demonstration of an inverted-grown, fully processed, thin-film, $Al_{0.34}Ga_{0.66}As/GaAs$ cascade solar cell. Also, AM1.5 cell efficiency of ~ 20.3% for a thin film GaAs cell has been obtained. An inverted-grown, thin-film, $Al_{0.34}Ga_{0.66}As/GaAs$ cascade with an efficiency of 19.9% at AM1.5 and an efficiency of 21% under ~ 7 AM1.5 suns, has been obtained. The thin-film approach based on a *sacrificial* Ge substrate and the eutectic-metal-bonding onto Si, has demonstrated a minority carrier lifetime of 103 ns, the highest for a GaAs thin film on Si. Based on internal quantum efficiency measurements, an electron diffusion length of ~ 7.0 μm has been estimated in the p-type base of an EMB thin-film GaAs cell on Si.

In conclusion, the inverted-growth approach to high-efficiency AlGaAs/GaAs cascade should allow a significant IR-transmission below GaAs bandgap. This can be used to mechanically stack the AlGaAs/GaAs cascade onto a moderately high-efficiency Si cell. The EMB scheme described in this effort can be modified to produce a 3-junction, 2-terminal, current-matched (at AM1.5), monolithic $Al_{0.37}Ga_{0.63}As/GaAs/Si$ cascade. Efficiency under (200X) concentration for such a cascade is projected to approach 40%. Most importantly, this approach will involve rather inexpensive Si cells, and the OMVPE growth of III-V cascades on potentially cheaper, large-area Ge substrates. It is worth noting that a significant cost (~ 70%) in the fabrication of the high-efficiency GaAs cells by OMVPE is from the GaAs substrates [20]. Thus the approach suggested in this program is likely to offer solutions to meet the long-term goals of NREL in the area of cost-effective, high-efficiency photovoltaics.

9.0 PUBLICATIONS

This NREL-funded research has resulted in the following publications over the past year:

1. R. Venkatasubramanian, M.L. Timmons, T.S. Colpitts and J.S. Hills, "Advances in the development of any AlGaAs/GaAs cascade solar cell using a patterned germanium tunnel interconnect", Solar Cells, 30, 345 (1991).

2.. R. Venkatasubramanian, M.L. Timmons, and T.S. Colpitts, "High Conductance GaAs Tunnel Diodes by OMVPE", Proc. of MRS Symposium on Atomic Layer Growth and Processing, April 1991, Anaheim, CA.

3. R. Venkatasubramanian, M.L. Timmons, and T.S. Colpitts, " Selective plasma etching of Ge substrates for thin freestanding GaAs-AlGaAs heterostructures", Appl. Phys. Lett., 59, 2153 (1991).

4. R. Venkatasubramanian, M.L. Timmons, T.P. Humphreys, B.M. Keyes, and R.K. Ahrenkiel, "High-Quality Eutectic-Metal-Bonded GaAs-AlGaAs Thin Films on Si Substrates", Appl. Phys. Lett., 60, 886 (1992).

5. R. Venkatasubramanian, M.L. Timmons, T.S. Colpitts, J.S. Hills, and J.A. Hutchby, "An Inverted-Growth Approach to Development of an IR-Transparent, High-Efficiency, AlGaAs/GaAs Cascade Solar Cell", Proc. of 22nd IEEE PVSC (IEEE Press, New York, NY, 1991), p. 93.

6. R. Venkatasubramanian, M.L. Timmons, T.S. Colpitts, and S. Asher, "Properties and Use of "Cycled" OMVPE GaAs:Zn, GaAs:Si, and GaAs:Se Layers for High-Conductance GaAs Tunnel Junctions", J. Elect. Mater. **21**, 893 (1992).

7. R. Venkatasubramanian, M.L. Timmons, P.R. Sharps, T.S. Colpitts, J. S. Hills, J. Hancock, and J.A. Hutchby, "Development of an IR-Transparent, Inverted-Grown, Thin-Film, $Al_{0.34}Ga_{0.66}As$/GaAs Cascade Solar Cell", Presented at the NREL PV AR&D 11th Review Meeting, May 14, 1992, Denver, Co.

8. R. Venkatasubramanian, M.L. Timmons, T.P. Humphreys, "Vertical-Cavity Fabry-Perot Action in µm-thick, Eutectic-Metal-Bonded (EMB) AlGaAs-GaAs Films on Si Substrates", Presented at the Electronic Materials Conference, June 26, 1992, Cambridge, MA.

10. REFERENCES

1. Chung, G.F. Virshup, S. Hikido, and N.R. Kaminar, Appl. Phys. Lett., **55**, 1741 (1989).

2. R. Venkatasubramanian, M.L. Timmons, T.S. Colpitts, and J.S. Hills, Solar Cells, **30,** 345 (1991).

3. R. Venkatasubramanian, M.L. Timmons, and T.S. Colpitts, Appl. Phys. Lett., **59,** 2153 (1991).

4. E. Yablonovitch, T. Gmitter, J.P. Harbison, and R. Bhat, Appl. Phys. Lett., **51**, 2222 (1987).

5.. R.K. Ahrenkiel, D.J. Dunlavy, J. Benner, R.P. Gale, R.W. McClelland, J.V. Gormley, and B.D. King, Appl. Phys. Lett., **53**, 598 (1988).

6. R.J. Pearah, W.T. Masselink, J. Klem, T. Henderson, H. Morkoc, C.W. Litton and D.C. Reynolds, Phys. Rev. B, **32**, (1975).

7. H.H. Berger, J. Electrochem. Soc., **119**, 507 (1972).

8. S.K. Ghandhi, R.T. Huang, and J.M. Borrego, Appl. Phys. Lett., **48**, 415 (1986).

9. D.L. Miller, S.W. Zehr, and J.S. Harris, Jr., J. Appl. Phys., **53**, 744 (1982).

10. C. Amano, H. Sugiura, A. Yamamoto, and M. Yamaguchi, Appl. Phys. Lett., **51**, 1998 (1987).

11. P.A. Iles, Y.M. Yeh, F.H. Ho, C.L. Chu, and C. Cheng, IEEE Elec. Dev. Lett., **11**, 140 (1990).

12. R. Venkatasubramanian, M.L. Timmons, T.P. Humphreys, B.M. Keyes, and R.K. Ahrenkiel, Appl. Phys. Lett., **60**, 886 (1992).

13. S.K. Ghandhi, *VLSI Fabrication Principles* (Wiley, New York, 1982), pp. 58-72.

14. Y.H. Lo, R. Bhat, D.M. Hwang, M.A. Koza, and T.P. Lee, Appl. Phys. Lett., **58**, 1961 (1991).

15. T.P. Humphreys, J.B. Posthill, K. Das, C.A. Sukow, R.J. Nemanich, N.R. Parikh, and A. Majeed, Jpn. J. Appl. Phys., **28**, L1595 (1989).

16. R.J.M. Griffiths, I.D. Blenkinsop, and D.R. Wright, Electron. Lett., **15**, 629 (1979).

17. R. Venkatasubramanian, M.L. Timmons, J.B. Posthill, B.M. Keyes, and R.K. Ahrenkiel, J. Cryst. Growth, **107**, 489 (1991).

18. R.F. McQuat and D.L. Pulfrey, in Proc. of the 11th IEEE Photovoltaic Specialists Conference, (IEEE, New York), 371 (1975).

19. S.M. Sze, *Physics of Semiconductor Devices*, 2nd Ed., John Wiley, New York, (1982).

20. S. Hogan, "GaAs Concentrator Cell Production Cost Analysis". Paper presented at the NREL PV AR&D 11th Review Meeting, Denver, CO, May 1992.

11. APPENDIX 1

Properties and Use of Cycled Grown OMVPE GaAs:Zn, GaAs:Se, and GaAs:Si Layers for High-Conductance GaAs Tunnel Junctions

R. Venkatasubramanian, M.L. Timmons, and T.S. Colpitts,

Research Triangle Institute, Research Triangle Park, NC 27709.

S.Asher,

National Renewable Energy Laboratory, Golden, CO 80401.

November 20, 1991

gaastunnelpaper

Abstract:

Heavily doped GaAs layers for high conductance GaAs tunnel junctions have been grown by atmospheric pressure organometallic vapor phase epitaxy (OMVPE) using Zn as the dopant for the p^+ regions and either Se or Si as the dopant for the n^+ regions. At a growth temperature of 700°C using a "cycled" growth technique for the Zn-doped p^{++}-GaAs layer, both the conductance and the peak current density of the tunnel diode has been increased by a factor of $\sim$ 65 compared to a tunnel junction with a continuously grown Zn-doped p^+- GaAs. The conductance of the tunnel junction, which is maximized at a growth temperature of 650°C using cycled growth, is comparable to the best reported values for tunnel junctions grown by molecular beam epitaxy. Cycled growths for n^+ Se-doped regions are found to reduce the conductance of a tunnel junction by more than two orders of magnitude. However, cycled growth for the n^+-GaAs regions with Si doping show conductance degradation. A model based on incorporation sites of these dopants during OMVPE growth of GaAs is presented to account for the experimental observations.

Key words: GaAs Tunnel Junctions, OMVPE, Cycled Growth

INTRODUCTION

Tunnel junctions are useful as interconnects in multijunction cascade solar cells. Monolithic cascade solar cells, based on lattice matched material systems such as $Al_xGa_{1-x}As/GaAs$ [1] and $Ga_{0.5}In_{0.5}P/GaAs$ [2], offer the promise of high-efficiency conversion for photovoltaic power systems. A key for these high efficiency multijunction solar cells is to develop a high conductance interconnect using a GaAs tunnel junction. GaAs tunnel junctions can also serve as active loads in GaAs FET logic circuits and as memory elements. The advantages of tunnel diode load circuits result from the large load capacitance introduced by the heavily doped p-n junction, which make them insensitive to increase in capacitance as a result of external sources as in multiple fan-outs. Thus, the tunnel diode load circuit can be faster for large fan-outs [3].

A discussion of the I-V characteristics of a tunnel diode is given elsewhere [4]. For the purposes of this paper, the specific resistivity of the tunnel diode is defined as the inverse of the ratio of the peak current density (J_p) to the voltage (V_p) across the diode at J_p. In addition, the nature of the peak to valley ratios of the current density (J_p/J_v) and the corresponding voltage ratio (V_p/V_v) controls its utility in some applications.

An important feature of a tunnel junction current-voltage (I-V) characteristic is the excess current [4]. This is the current component that exceeds the tunneling and diffusion current existing in a forward-biased p^+-n^+ junction. The excess current can

reduce the (J_p/J_v) ratio, thus reducing the negative differential region (NDR) in the I-V characteristic. While the lack of a well pronounced NDR makes the tunnel diode unsuitable for digital applications, it is tolerable for interconnect applications in multi-junction solar cells. The excess current arises from band-tail tunneling between the p^+- and n^+-regions, which result from heavy doping, and also from tunneling through mid-gap states.

In this paper we present results on conductance and the NDR behaviour of GaAs p^+ - n^+ tunnel junctions grown by atmospheric-pressure OMVPE. Zinc is the dopant for the p^+ regions, and either Se or Si as the dopant for the n^+ regions. An approach denoted as "cycled" growth is examined and has been shown to improve the conductance of the tunnel junctions under certain doping conditions. The material properties of cycled-grown GaAs:Zn, GaAs:Se, and GaAs:Si are discussed first, to explain the tunnel junction results.

EXPERIMENTAL

The GaAs tunnel junctions were grown in a conventional atmospheric-pressure OMVPE growth system using trimethylgallium (TMGa) and arsine (AsH_3). The growth temperature range considered in this study was between 650-700 °C. The AsH_3/TMGa ratio was typically 30, and the H_2 carrier flow rate was 8 slm. Dimethylzinc (DMZn) was used for p-type doping. Silane (SiH_4) was used to obtain Si doping and hydrogen selenide (H_2Se) was used for Se doping. A schematic of the growth procedure in the

case of "cycled" growth is indicated in Figure 1. With this technique, AsH_3 and the respective dopant flows were uninterrupted while the TMGa flow was introduced periodically. The TMGa on-time was about 7 seconds and the off-time was about 13 seconds. The growth rate employed during the on-cycle was about 5 Å/s, the same as that in a continuously-grown layer.

GaAs:Zn, GaAs:Se, and GaAs:Si layers on semi-insulating GaAs substrates were used in this study. Material characterization techniques employed, include the Hall technique for free-carrier concentration, secondary ion mass spectrometry (SIMS) for the total dopant levels, and 300K photoluminescence (PL) to study the effects of cycled growth on luminescence characteristics. The free carrier concentration was obtained using the van der Pauw technique at a magnetic field of 5 kG. The layer thicknesses for the Hall data were obtained from the SIMS data, discussed below. A 0.1-μm-thick $Al_{0.8}Ga_{0.2}As$ surface-layer with the same doping level as in the respective GaAs layers, was used to reduce the effects of front-surface recombination during PL measurements. PL was performed on a conventional system using the 5145-Å line of an Ar ion laser.

The total Zn, Si and Se concentrations in the layers were obtained by SIMS using a Cameca 3f system. The SIMS profiles obtained on both the continuously-grown and cycled-grown GaAs:Zn, GaAs:Se, and GaAs:Si layers are shown in Fig. 2, 3, and 4, respectively. The depth profiles were obtained from measured sputtered rates on GaAs calibration samples. The broad dopant spike/anomaly seen near the surface in the

SIMS data in Figs. 2 to 4, is a result of dopant incorporation in the $Al_{0.8}Ga_{0.2}As$ surface-layer being different from that in the GaAs layer. We also note that the dopant spread at the substrate-epi interface region (in Figs. 2 to 4), probably a result of diffusion effects, is at concentrations ~100 lower than the respective average doping level in the bulk of the layer. Also, the growth time for the actual tunnel junction layers are about one-tenth of those for layers grown for SIMS data in Figs. 2 to 4. Thus the effect of diffusion of dopants in the characteristics of tunnel junctions, discussed below, can be considered marginal at best.

A schematic cross section of a typical tunnel junction with various layer thicknesses, is shown in Figure 5. The tunnel diode area is 9 x 10^{-4} cm^2. The specific contact resistance of the AuGe/Ni/Au (500Å/150Å/2000Å) multilayer metallization to the n^+-GaAs substrate, sintered at 350°C for 30 s, was measured to be less than 1 x 10^{-4} ohm-cm^2. This specific contact resistance is about a factor of thirty lower than the lowest specific contact resistance obtained for the best GaAs tunnel junction in this work. The specific resistivity of non-sintered Ti/Au (500Å/2000Å) metallization to p^+-GaAs was measured to be 6 x 10^{-6} ohm-cm^2. These contact resistivities were obtained from transmission line model (TLM) patterns [5].

RESULTS AND DISCUSSION

The Hall carrier data, the total Zn level obtained from SIMS (Fig. 2), and the 300K photoluminescence (PL) peak energies, of GaAs:Zn using continuous and cycled growths are indicated in Table 1. Here the DMZn partial pressure and the growth

temperature were kept constant at about 0.4 Torr and 700 ° C, respectively, for both the growth cases. The hole concentration level has fallen by a factor of two in the cycled-grown GaAs. The SIMS data, however, indicates that the total amount of zinc in the cycled and continuously grown layers is about the same. Thus, we note a significant increase in compensation of the cycled-grown GaAs:Zn. The lower PL peak energy in the cycled-growth sample in spite of the lower hole concentration is noteworthy.

We believe that, during the off-cycle of the cycled-grown GaAs:Zn, the simultaneous presence of AsH_3 and DMZn over the GaAs surface results in the preferential adsorption of Zn onto interstitial lattice-sites. (A model for interstitial adsorption of dopant atoms such as sulfur on a GaAs surface during OMVPE has been modelled elsewhere [6].) Following the off-cycle, when GaAs growth is initiated, the Zn adatoms are probably trapped on the interstitial sites. The interstitial Zn (Zn_i) is expected to be a donor in GaAs [7] and, therefore, can cause n-type compensation of the p^+-type material, resulting in a lower hole concentration. Further, the presence of Zn_i donors near the valence-band edge [7] can cause the overlap of the interband transition and the conduction-band to Zn_i donor transition, causing the PL peak energy to shift to lower energies.

In GaAs:Zn grown by OMVPE, it has been shown that Zn incorporation increases (as measured by hole concentration) with the growth rate of GaAs. This behaviour has been explained by a trapping mechanism [8]. It is also likely, for a given Zn-overpressure and adsorption rate on the GaAs surface, that beyond a certain amount

of substitutional Zn incorporation, some interstitial incorporation occurs. The fraction of interstitial incorporation is likely to become significant at high Zn overpressures. The interstitial Zn donors can, therefore, cause compensation and the hole concentration may be lowered. With a higher growth rate one might expect a higher substitutional incorporation, leading to a higher hole concentration.

The material characteristics of GaAs:Se using continuous and cycled growths are indicated in Table 2. Here the H_2Se partial pressure and the growth temperature were kept constant at about 0.015 Torr and 700 °C, respectively. The electron concentration is similar in both cases of growth. The 300K PL peak energy of the continuously grown GaAs:Se with a slightly higher free carrier concentration is higher than that of the cycled grown sample. This is expected because of the increased bandfilling effects with a higher free electron concentration. However, the relative PL intensity of the cycled grown GaAs:Se is about 4-5 times higher than that of the continuously grown GaAs:Se. This suggests that the non-radiative processes are weaker in the cycled grown GaAs:Se and it is likely that V_{Ga}-Se_{As} deep level complexes, which are known to occur in heavily doped n-GaAs [9,10], are thermally annealed out during the off cycle of the cycled growth. The thermal annealing of such deep levels and their consequent effects on lifetime (in turn on PL intensity) have been previously noted [11]. In effect, we observe that continuously grown GaAs:Se is likely to have a larger concentration of V_{Ga}-Se_{As} deep levels than the cycled grown GaAs:Se. This argument will be further discussed below to interpret some of the tunnel junction data.

The Hall carrier data, total Si concentration from SIMS, and 300K PL characteristics of Si:GaAs using regular and cycled growths are indicated in Table 3. The net free carrier concentration in either growth case are about the same. However, the mobility of the cycled grown GaAs:Si is significantly lower than that of the continuously grown GaAs:Si suggesting increased compensation with cycled growth. This is also evident from the compensation ratio deduced from SIMS and the Hall carrier data. Further the 300K PL peak energy of the cycled grown sample is significantly lower than that of the continuously grown sample in spite of a very similar net free carrier concentration.

Both these observations are explained well by increased Si_{As}-acceptor compensation in the cycled grown GaAs:Si. Si incorporation onto As sites during the off cycle is probably a result of less-than-exact-unity As coverage on the GaAs surface. It has been shown that Si_{As} is the dominant acceptor compensator in heavily doped GaAs:Si grown by OMVPE [12], with a negligible role of V_{Ga}-Si_{Ga} acceptor complexes. Thus, the thermal annealing during cycled-growth is not expected to introduce any effect on near-band-edge PL intensity. The data in Table 3 show this.

The characteristics of GaAs tunnel diodes with continuous growth for GaAs:Se and either continuous or cycled growth for GaAs:Zn are shown in Fig. 6a and 6b, respectively. The peak current density (J_p) of the tunnel junction with the cycled GaAs:Zn is larger by a factor of about 65 and the specific resistance is correspondingly smaller by the same amount than that of the junction with continuously grown GaAs:Zn. The increase in conductance (Fig. 6b) is also accompanied by the

disappearance of a well-marked NDR (in Fig. 6a). By plotting the J_p values versus effective doping concentration (as discussed in Ref. 13) for both cases, we find that J_p in Fig. 6a is smaller than the theoretical value by a factor of two, while the J_p in Fig. 6b, is higher than the theoretical value by about two orders of magnitude. We note that the GaAs tunnel junction grown with both cycled GaAs:Zn and GaAs:Se regions has the NDR (Fig. 6c) and a J_p value consistent with the theoretical value based on doping levels.

Similar improvements in J_p and the conductance of the tunnel junctions with cycled GaAs:Zn regions were observed at a growth temperature of 650 °C (Table 4). However, the increase in J_p was ~50 compared to ~65 seen at a growth temperature of 700 °C. At a growth temperature of 650 °C, we have obtained a J_p of 12.8 A / cm^2 and a specific contact resistance of 3.3 x 10^{-3} ohm-cm^2. This is comparable to the smallest reported value of 3.0 x 10^{-3} ohm-cm^2 for a GaAs tunnel junction grown at 520 °C, by molecular beam epitaxy [14].

Using a cycled GaAs:Zn layer in a GaAs tunnel junction with Si as the dopant for the n^+-region leads to a reduction in J_p and the specific-resistance, mainly as a result of the decrease in hole concentration in the cycled GaAs:Zn. The I-V characteristics of tunnel junctions with GaAs:Si for the n^+-regions, using continuous growth or cycled growth for GaAs:Zn, are indicated in Fig. 7a and 7b, respectively. The NDR is pronounced in both I-V characteristics; this contrasts with those shown in Fig. 6a and 6b. It has also been observed that the J_p values were within about 20-30 percent of the

theoretical values for the respective doping levels. The cycled growth of GaAs:Si did not affect the J_p and the conductance values, whether a cycled or continuous GaAs:Zn layer was used to make the tunnel junction.

We can explain the tunnel junction results in terms of the earlier discussed material properties, as follows. In the case of tunnel diodes with GaAs:Se (continuous) and GaAs:Zn (cycled) doping, the presence of V_{Ga}-Se_{As} defects in the n^+-GaAs region and Zn_i in the p^+-GaAs region assist in extra carrier tunneling. Thus, J_p is about two orders of magnitude higher than the theoretical value, and the NDR disappears as a result of this excess current. However, with a cycled GaAs:Se layer for n^+-GaAs, the concentration of V_{Ga}-Se_{As} centers are probably low due to thermal annealing. Thus, even though Zn_i defects are likely in the p^+-GaAs side of the tunnel junction, there are probably no accompanying states in the n^+-GaAs to complete the carrier tunneling. Thus, the GaAs tunnel junction with cycled GaAs:Se and GaAs:Zn layers show NDR, as well as a J_p close to the theoretical value for the doping level.

In the case of GaAs:Si and GaAs:Zn system, the low levels of Si_{Ga}-V_{Ga} complexes in Si:GaAs probably limit extra carrier tunneling even though Zn_i defects are present in the cycled Zn:GaAs region. Hence, we obtain near ideal J_p values which are consistent with the doping levels under all conditions of growth of GaAs tunnel junctions with Si doping for the n^+-GaAs region.

SUMMARY

We have examined an approach denoted as "cycled" growth in conventional OMVPE. At a growth temperature of 700 °C using a cycled growth for the Zn doped p^{++}-GaAs layer, both the conductance and the peak current density of the tunnel diode has been increased by a factor of $\sim$65 compared to a tunnel junction with continuous growth for the Zn-doped layer. The conductance of the tunnel junction with cycled growth is apparently maximized at a growth temperature of 650 °C. Cycled growth for n^{+}-GaAs region with the Se-doping is found detrimental for the tunnel junction conductance. However, cycled growth for the n^{+}-GaAs region with Si-doping does not lead to conductance degradation. The material characteristics of cycled grown OMVPE GaAs:Zn, GaAs:Se, and GaAs:Si layers are also presented. A model based on the incorporation sites of these dopants during OMVPE of GaAs is described to account for both the observed material properties and the tunnel junction characteristics.

ACKNOWLEDGMENT

This work was supported by National Renewable Energy Laboratory under Subcontract No. XM-0-18110-2 with Mr. T.S. Basso as the technical monitor.

References

1. S.M. Bedair, J.A. Hutchby, J.P.C. Chiang, M. Simons, and J.R. Hauser, Proc. of the 15th IEEE Photovoltaic Specialists Conf. (IEEE, New York, 1982), p.692.

2. J.M. Olson, S.R. Kurtz, A.E. Kibbler, and P. Faine, Appl. Phys. Lett. 56, 623 (1990).

3. J.V. DiLorenzo and D.D. Khandelwal, "GaAs FET Principles and Technology", Artech House, Dedham, Massaschsetts, 646 (1982).

4. S.M. Sze, "Physics of Semiconductor Devices", 2nd Edition, John Wiley, New York, 517 (1981).

5. H.H. Berger, J. Electrochem. Soc., 119, 507 (1972).

6. R.J. Field and S.K. Ghandhi, J. Cryst. Growth, 74, 551 (1986).

7. A. Luque, J. Martin, and G.L. Arujo, J. Electrochem. Soc., 123, 249 (1976).

8. T.F. Kuech, M.A. Tischler, R. Potemski, F. Cardone, and G. Scilla, J. Cryst. Growth, 98, 174 (1989).

9. D.T.J. Hurle, J. Phys. Chem. Solids, 40, 627 (1979).

10. R. Venkatasubramanian, S.K. Ghandhi, and T.F. Kuech, J. Cryst. Growth, 97, 827 (1989).

11. G. Mathur, M.L. Wheaton, J.M. Borrego, and S.K. Ghandhi, J. Appl. Phys. 57, 4711 (1985).

12. R. Venkatasubramanian, K. Patel and S.K. Ghandhi, J. Cryst. Growth, 94, 34 (1989).

13. S.K. Ghandhi, R.T. Huang, and J.M. Borrego, Appl. Phys. Lett., 48, 415 (1986).

14. D.L. Miller, S.W. Zehr, and J.S. Harris, Jr., J. Appl. Phys., 53, 744 (1982).

Figure Captions

Figure 1. Schematic of the "cycled" growth procedure.

Figure 2. SIMS profile of GaAs:Zn grown using continuous and cycled growth.

Figure 3. SIMS profile of GaAs:Se grown using continuous and cycled growth.

Figure 4. SIMS profile of GaAs:Si grown using continuous and cycled growth.

Figure 5. Schematic cross section of the GaAs tunnel diode indicating various layer thicknesses and ohmic contacts.

Figure 6. I-V characteristics of GaAs tunnel junctions grown with continuous growth for GaAs:Se, and a) continuous and b) cycled growth for GaAs:Zn. Shown in (c) is the I-V characteristic for a tunnel junction with cycled growth for GaAs:Se and GaAs:Zn.

Figure 7. I-V characteristics of tunnel junctions with GaAs:Si for the n^+-regions and (a) continuous growth and (b) cycled growth for GaAs:Zn.

TABLE 1

Material characteristics of GaAs:Zn using continuous and cycled growths at 700 ° C.

	Continuous Growth	Cycled Growth
SIMS Zn Concentration (cm^{-3})	3.3×10^{19}	3.0×10^{19}
Hole Concentration (cm^{-3})	3.1×10^{19}	1.5×10^{19}
Hole Mobility (cm^2/V sec)	56	66
Compensation Ratio (N_D^+/N_A^-)	0.06	0.5
300K PL Peak Energy (eV)	1.414	1.397

Relative PL intensities of the band-edge emission in both samples are comparable.

TABLE 2

Material characteristics of GaAs:Se using continuous and cycled growths at 700 ° C.

	Continuous Growth	Cycled Growth
SIMS Se Concentration (cm^{-3})	3.2×10^{19}	4.5×10^{19}
Electron Concentration (cm^{-3})	6.6×10^{18}	6.1×10^{18}
Electron Mobility (cm^2/V sec)	1034	915
Compensation Ratio (N_A^-/N_D^+)	0.66	0.76
300K PL Peak Energy (eV)	1.445	1.434

Relative PL intensity of band-edge emission in cycled GaAs:Se is 4-5 times larger than that of continuously grown GaAs:Se.

TABLE 3

Material characteristics of GaAs:Si using continuous and cycled growths at 700 ° C.

	Continuous Growth	Cycled Growth
SIMS Si Concentration (cm^{-3})	1.2×10^{19}	3.5×10^{19}
Electron Concentration (cm^{-3})	4.9×10^{18}	4.3×10^{18}
Electron Mobility (cm^2/V sec)	1237	922
Compensation Ratio (N_A^-/N_D^+)	0.42	0.78
300K PL Peak Energy (eV)	1.484	1.426

Relative PL intensities of the band-edge emission in both cases are comparable.

TABLE 4

Peak tunnel current density of GaAs tunnel junctions at different growth temperatures, using continuous and cycled growths for GaAs:Zn.

Growth Temperature (°C)	J_p of Tunnel Diode (mA/cm^2) GaAs:Se Continuous	
	Zn: Continuous	Zn: Cycled
700	47	3000
650	256	12800*

* Specific resistance of 3.3×10^{-3} ohm - cm^2

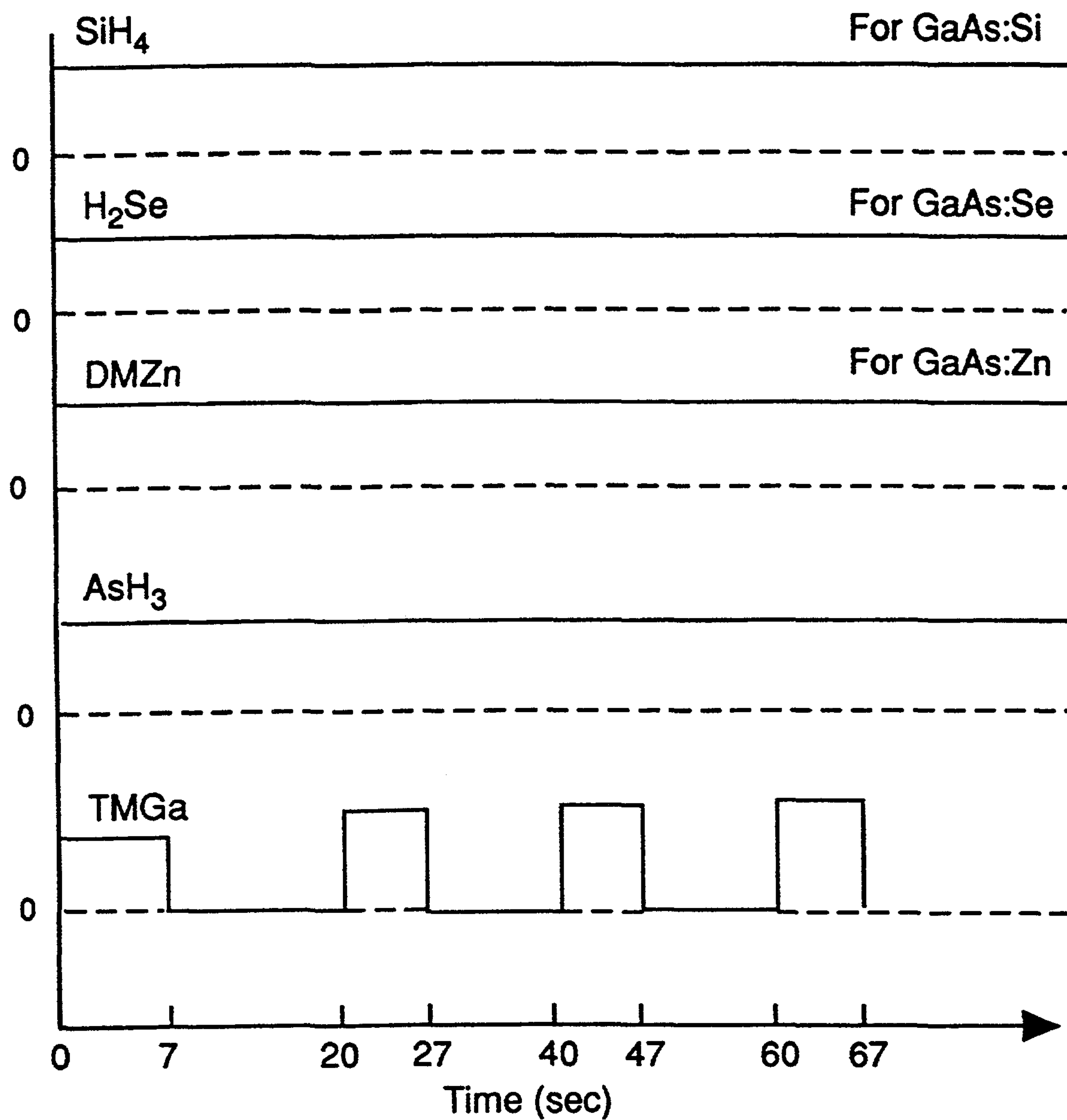

FIG 1/RVE

Depth Profile for Zn

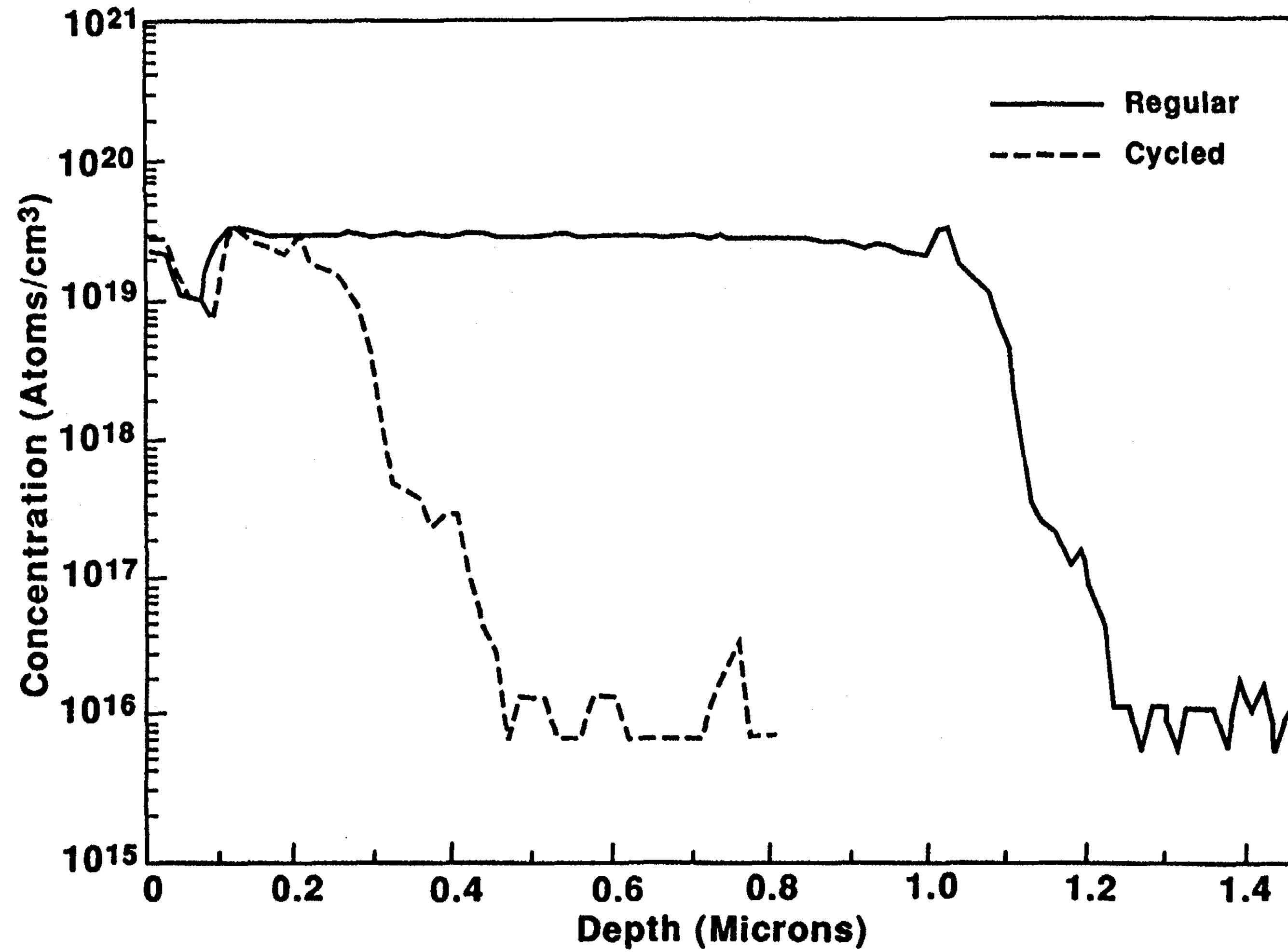

Depth Profile for Se

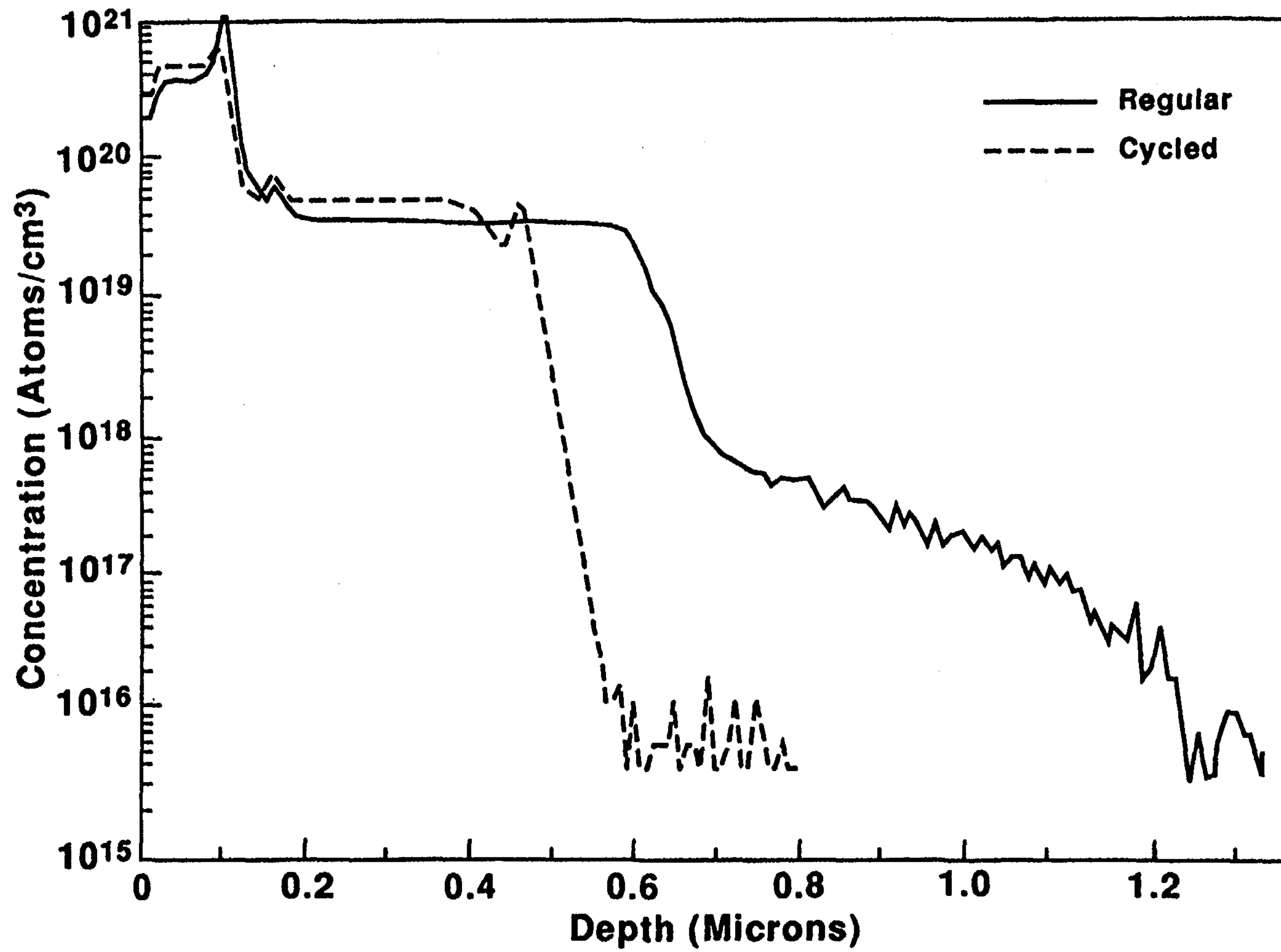

Depth Profile for Si

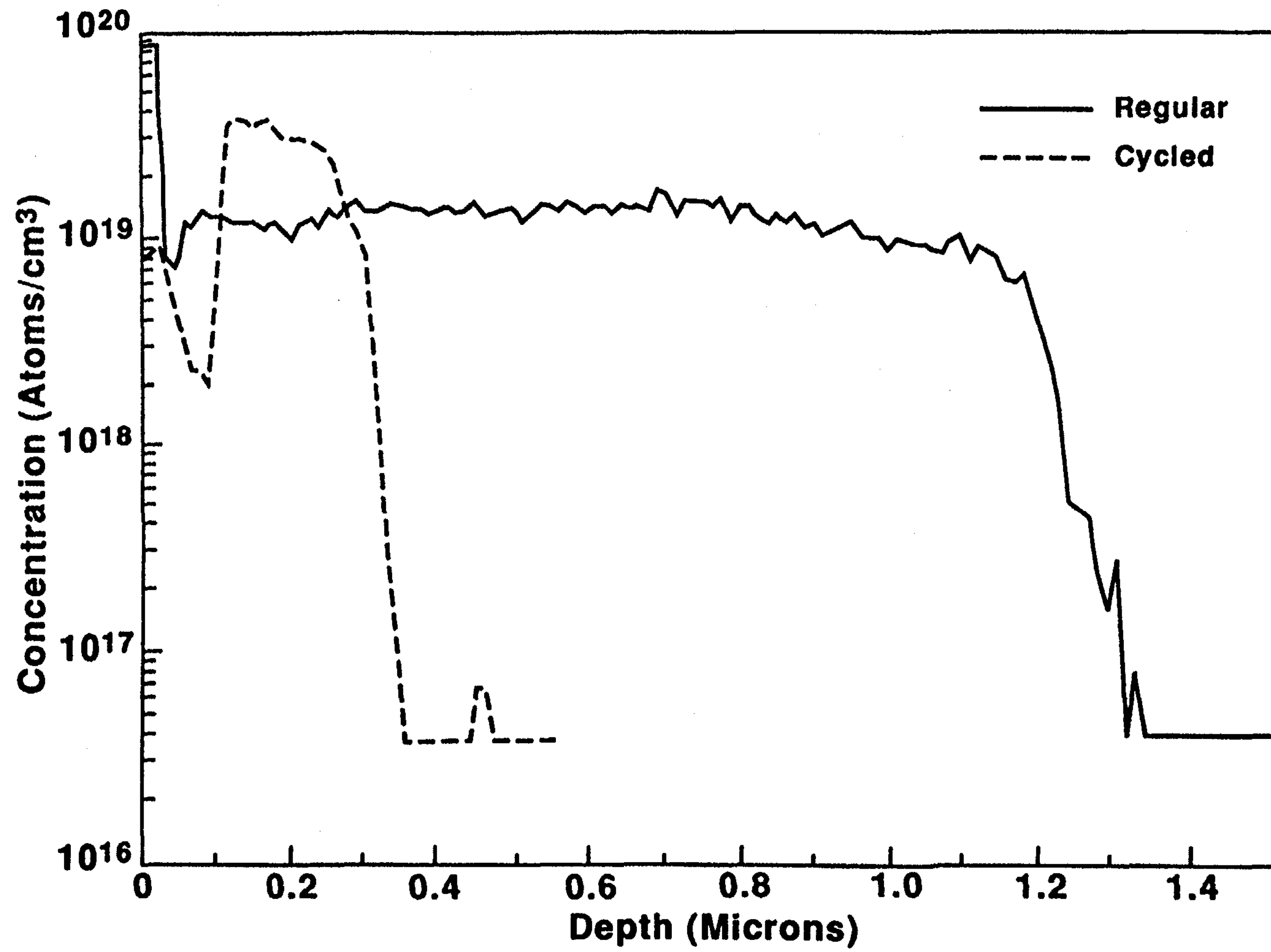

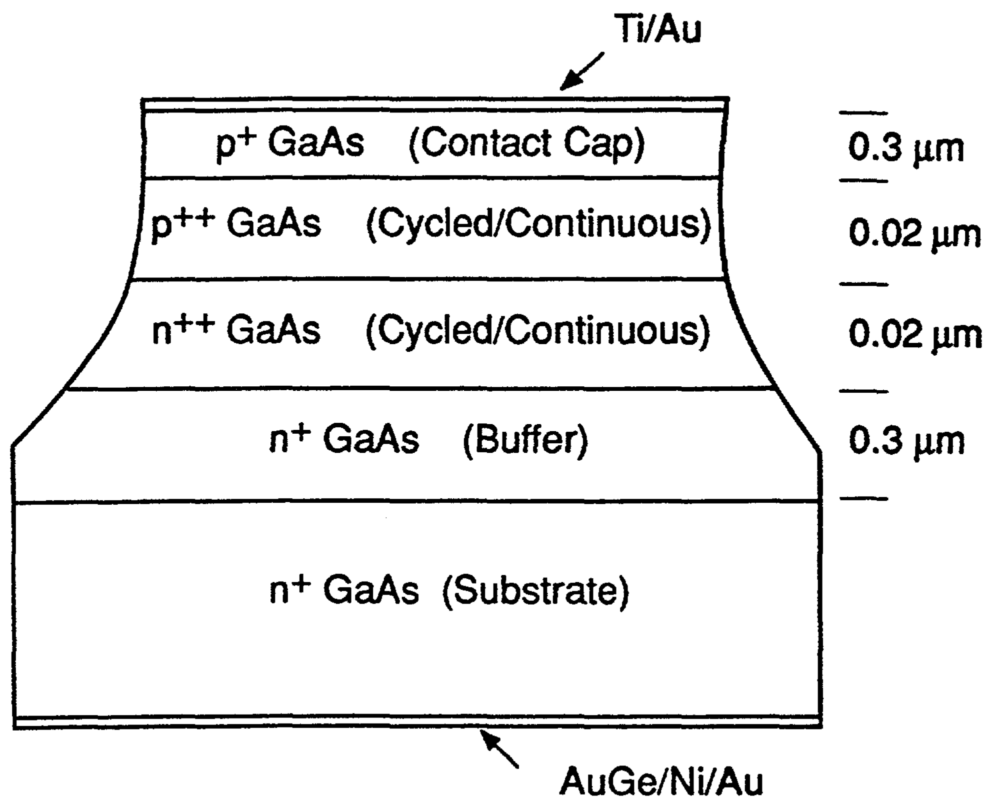

FIG. 5/RV

H: 0.5 V/div.   V: 20 μA/div.

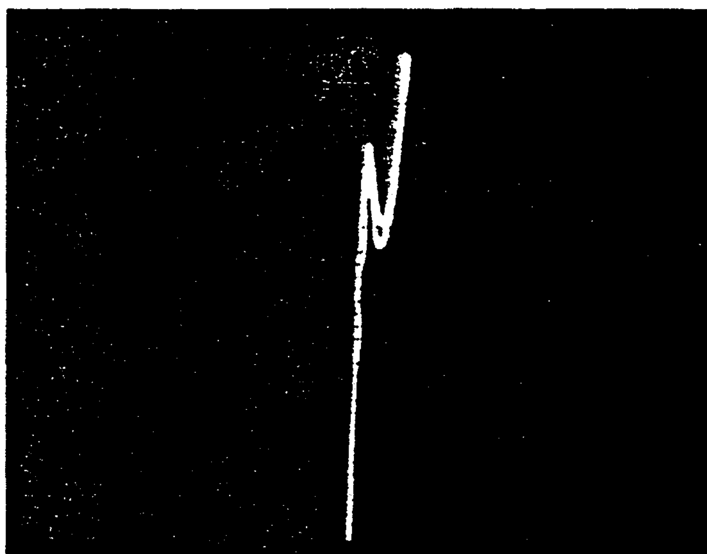

(a)

H: 0.1 V/div.   V: 2 mA/div.

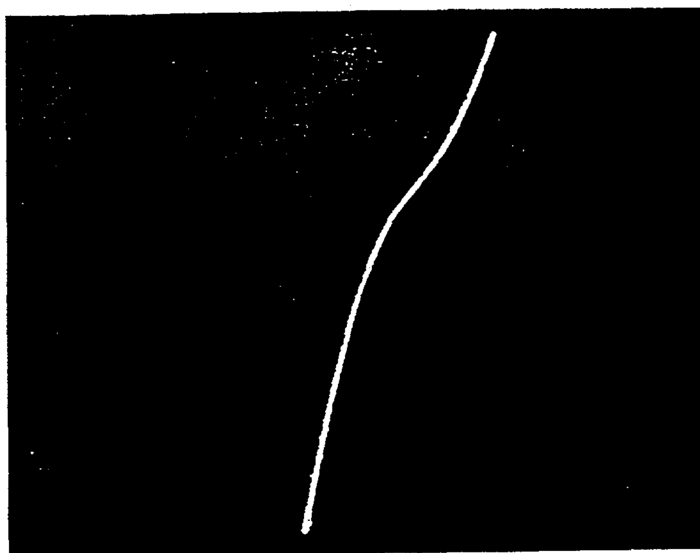

(b)

FIG6/RV etc

H: 0.5 V/div.   V: 20 μA/div.

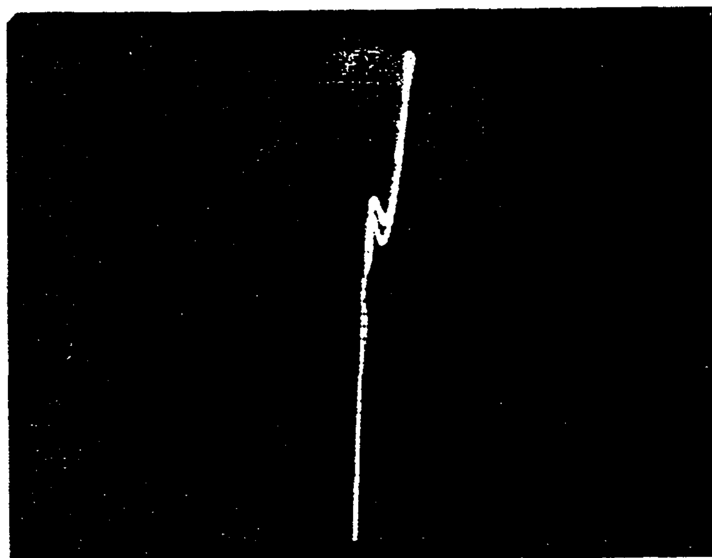

(c)

FIG 6/2ve

H: 0.5 V/div. V: 20 μA/div.

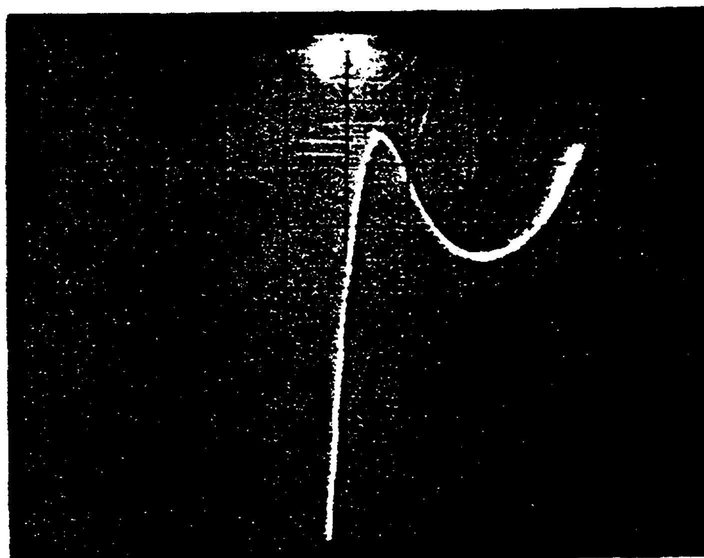

(a)

H: 0.5 V/div. V: 20 μA/div.

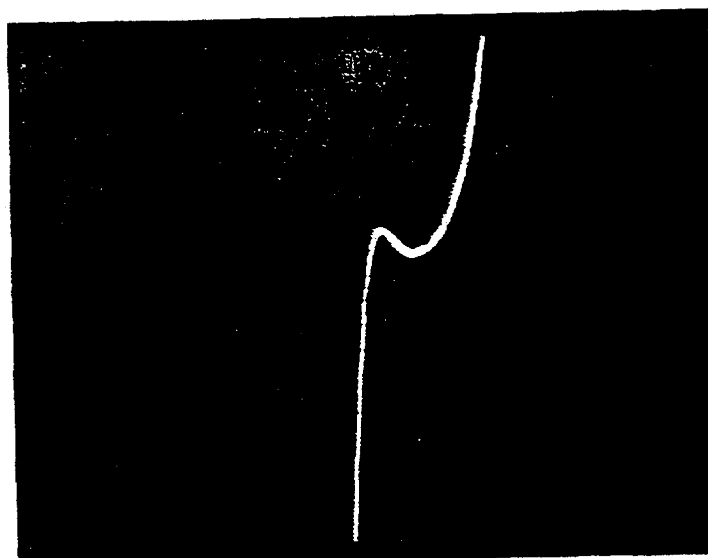

(b)

FIG 7/RV et

Document Control Page	1. NREL Report No.	2. NTIS Accession No.	3. Recipient's Accession No.
	NREL/TP-411-5289	DE93000073	

4. Title and Subtitle

An Inverted AlGaAs/GaAs Patterned-Ge Tunnel Junction Cascade Concentrator Solar Cell

5. Publication Date
January 1993

6.

7. Author(s)
R. Venkatasubramanian

8. Performing Organization Rept. No.

9. Performing Organization Name and Address

Research Triangle Institute
P.O. Box 12194
Research Triangle Park, NC 27709-2194

10. Project/Task/Work Unit No.
PV221104

11. Contract (C) or Grant (G) No.

(C) XM-0-18110-2

(G)

12. Sponsoring Organization Name and Address
National Renewable Energy Laboratory
1617 Cole Blvd.
Golden, CO 80401-3393

13. Type of Report & Period Covered

Technical Report
1 January 1991 - 31 August 1992

14.

15. Supplementary Notes
NREL technical monitor: T.S. Basso

16. Abstract (Limit: 200 words)
This report describes work to develop inverted-grown $Al_{0.34}Ga_{0.66}As$/GaAs cascades. Several significant developments are reported on as follows: (1) The AM1.5 1-sun total-area efficiency of the top $Al_{0.34}Ga_{0.66}As$ cell for the cascade was improved from 11.3% to 13.2% (NREL measurement [total-area]). (2) The "cycled" organometallic vapor phase epitaxy growth (OMVPE) was studied in detail utilizing a combination of characterization techniques including Hall-data, photoluminescence, and secondary ion mass spectroscopy. (3) A technique called eutectic-metal-bonding (EMB) was developed by strain-free mounting of thin GaAs-AlGaAs films (based on lattice-matched growth on Ge substrates and selective plasma etching of Ge substrates) onto Si carrier substrates. Minority-carrier lifetime in an EMB GaAs double-heterostructure was measured as high as 103 nsec, the highest lifetime report for a freestanding GaAs thin film. (4) A thin-film, inverted-grown GaAs cell with a 1-sun AM1.5 active-area efficiency of 20.3% was obtained. This cell was eutectic-metal-bonded onto Si. (5) A thin-film, inverted-grown, $Al_{0.34}Ga_{0.66}As$/GaAs cascade with AM1.5 efficiency of 19.9% and 21% at 1-sun and 7-suns, respectively, was obtained. This represents an important milestone in the development of an AlGaAs/GaAs cascade by OMVPE utilizing a tunnel interconnect and demonstrates a proof-of-concept for the inverted-growth approach.

17. Document Analysis
a. Descriptors
concentrator ; tunnel junction ; gallium arsenide ; photovoltaics ; solar cells

b. Identifiers/Open-Ended Terms

c. UC Categories
275

18. Availability Statement
National Technical Information Service
U.S. Department of Commerce
5285 Port Royal Road
Springfield, VA 22161

19. No. of Pages
76

20. Price
A05

Form No. 0069E (6-30-87)